JAERI-M
92-145

OPTIMIZATION FOR STEADY-STATE AND HYBRID OPERATIONS OF ITER BY USING SCALING MODELS OF DIVERTOR HEAT LOAD

September 1992

Yoshiki MURAKAMI*, Hirobumi FUJIEDA**
Kiyoshi ITAMI and Masayoshi SUGIHARA

日本原子力研究所
Japan Atomic Energy Research Institute

JAERI-Mレポートは，日本原子力研究所が不定期に公刊している研究報告書です。
入手の問合わせは，日本原子力研究所技術情報部情報資料課（〒319-11茨城県那珂郡東海村）あて，お申しこしください。なお，このほかに財団法人原子力弘済会資料センター（〒319-11 茨城県那珂郡東海村日本原子力研究所内）で複写による実費頒布をおこなっております。

JAERI-M reports are issued irregularly.
Inquiries about availability of the reports should be addressed to Information Division, Department of Technical Information, Japan Atomic Energy Research Institute, Tokai-mura, Naka-gun, Ibaraki-ken 319-11, Japan.

© Japan Atomic Energy Research Institute, 1992

編集兼発行　日本原子力研究所
印　　刷　㈱原子力資料サービス

JAERI-M 92-145

Optimization for Steady-state and Hybrid Operations of ITER by using Scaling Models of Divertor Heat Load

Yoshiki MURAKAMI*, Hirobumi FUJIEDA**
Kiyoshi ITAMI+ and Masayoshi SUGIHARA

Department of ITER Project
Naka Fusion Research Establishment
Japan Atomic Energy Research Institute
Naka-machi, Naka-gun, Ibaraki-ken

(Received August 27, 1992)

Steady-state and hybrid mode operations of ITER are investigated by 0-D power balance calculations assuming no radiation and charge-exchange cooling in divertor region. Operation points are optimized with respect to divertor heat load which must be reduced to the level of ignition mode ($\sim$5 MW/m^2). Dependence of the divertor heat load on the variety of the models, i.e., constant-χ model, Bohm-type-χ model and JT-60U empirical scaling model, is also discussed. The divertor heat load increases linearly with the fusion power (P_{FUS}) in all models. The possible highest fusion power much differs for each model with an allowable divertor heat load. The heat load evaluated by constant-χ model is, for example, about 1.8 times larger than that by Bohm-type-χ model at P_{FUS} = 750 MW. Therefore, it should be important to refine the divertor scaling model. For these models assumed in this report, the fusion power for the steady-state mode should be smaller than about 200 $\sim$ 400 MW within the constraint such as the divertor heat load, helium accumulation (He = 10%), β-limit (Troyon $g \leq 3$), NBI power ($P_{NBI} \leq 120$ MW) and enhancement factor, H, of energy confinement time over L-mode scaling laws ($H \leq 2.1$). Effect of reduction of the helium accumulation, improvements of the

---

+ Department of Fusion Plasma Research
* On loan from Toshiba Corporation
** Atomic Data Service

confinement capability and the current-drive efficiency are also investigated aiming at lowering the divertor heat load. If Troyon g = 3.4, H = 2.5, He = 5% and 40% enhancement of the current-drive efficiency are achieved simultaneously, the divertor heat load can be reduced to the level of ignition mode without impurity seeding at P_{FUS} = 690 MW corresponding to neutron wall load of 1 MW/m^2 at the test region. Hybrid mode operation appears to be suitable for the technology testing that requires long burn time and high neutron wall load. It is found that NBI power should be larger than about 60 MW to obtain a burn time longer than 2000 s. The optimized operation point, where the minimum divertor heat load is achieved, does not depend on the model and is the point with the minimum-P_{FUS} and the maximum-P_{NBI}. When P_{FUS} = 690 MW and P_{NBI} = 110 MW, the divertor heat load can be reduced to the level of ignition mode without impurity seeding if H = 2.2 is achieved. Controllability of the current-profile is also discussed.

Keywords: Tokamak, ITER, Fusion Reactor, Steady-state Tokamak Operation, Divertor, Hybrid Tokamak Operation, H-factor, Troyon Coefficient, Fusion Burn Time

ＩＴＥＲにおける長時間および定常運転モードでのダイバータ熱負荷の比例則を用いた運転点の最適化

日本原子力研究所那珂研究所ＩＴＥＲ開発室
村上　好樹*・藤枝　浩文**・伊丹　潔+・杉原　正芳

（1992年８月27日受理）

国際熱核融合実験炉（ＩＴＥＲ）における長時間および定常運転動作点のシステム検討を行い，ダイバータ熱負荷の観点から運転点の最適化を行った。エネルギー閉じ込め則としてＩＴＥＲ89パワー則を用いると定常運転可能領域は核融合出力が増加するにつれて小さくなるが，ＩＴＥＲの装置パラメータでは約 750MWまで運転が可能である。しかし実際に運転が可能かどうかはダイバータ熱負荷の許容レベルによるため，与えられた核融合出力に対してダイバータ熱負荷を最小にする運転点を見いだし，その時の熱負荷のレベルを評価することが重要である。本研究では簡単な比例則を用いてダイバータ熱負荷を計算した。比例則としてはＩＴＥＲのガイドラインとなっている一定χ（熱拡散係数）モデルだけでなく，ボーム型のχモデル，ＪＴ－60Ｕの実験で得られた比例則を用い，モデルによる依存性も調べた。最適化された運転点におけるダイバータ熱負荷の核融合出力依存性を調べたところ，定常運転モードでのダイバータ熱負荷は核融合出力によって増加すること，その傾向はモデルによらず同様であるが，熱負荷の値は 750MWで約 1.8倍異なることがわかった。これは許容される熱負荷が与えられたとき運転可能な核融合出力がモデルによって大きく異なることを意味するので今後ダイバータ比例則の精密化が必要であろう。またヘリウム蓄積，閉じ込め，電流駆動効率の改善に対する効果を調べたところいずれも１～３割程度の熱負荷の改善が見られた。また不純物注入では放射損失によりダイバータ部流入パワーが減少するため熱負荷が数分の１に減少することがわかったが，主プラズマの閉じ込めに与える影響が未解明であるため今後の実験で明らかにしていく必要があろう。長時間運転モードでは，与えられた核融合出力と電流駆動パワーに対して到達可能最大燃焼時間を調べた。この場合，燃焼時間が工学試験で要求される時間（約2000秒）より長ければ，燃焼時間を2000秒まで短くすることにより，電子温度を下げてダイバータ熱負荷を減少させることができる。そうしてダイバータ熱負荷を最適化した結果，最適点は比例則に依存せず，核融合出力が小さいほど，電流

那珂研究所：〒311-01　茨城県那珂郡那珂町大字向山 801-1
+　炉心プラズマ研究部
*　㈱東芝より出向中
**　㈱原子力資料サービス

駆動パワーが大きいほど熱負荷が小さいことがわかった。また不純物添加を行わなくても閉じ込めを１割程度改善することで，熱負荷を自己点火モードと同程度にできることもわかった。

Contents

目　　次

1. Introduction

Conceptual Design Activities (CDA) of International Thermonuclear Experimental Reactor (ITER) were successfully completed in December 1990. In CDA phase, parametric and design space analysis has been extensively performed and the choice of the ITER baseline design and operation modes have been determined [1]. ITER operation modes are categorized into three groups, i.e., inductive (ignition mode) operations, long-pulse (hybrid mode) operations and steady-state mode operations. In each operation mode, the reference operation points are chosen to satisfy the several constraints such as beta limit, auxiliary heating power, energy confinement time, neutron wall load for technology testing, divertor heat load, etc. The ignition capability is shown to be reasonable and the hybrid operations with impurity seeding satisfy the required conditions [2]. So far, however, no steady-state operation with high neutron wall load satisfies the divertor constraint because of the low density necessary for efficient non-inductive current drive. In case of hybrid mode, the operation is possible, but the effect of impurity seeding on the confinement of main plasma is still unknown. Therefore, it is considered that the heat removal of the divertor plate is an important R & D issue and the further optimization of the operation points is necessary.

In this report, the operation point of ITER is analyzed by using a 0-D Tokamak Plasma Power Balance Calculation (TPC) code developed for ITER CDA. TPC code solves 0-D power balance of a tokamak plasma including profile effects and calculates beta values, Troyon coefficient, energy confinement time, neutron wall load, divertor heat load, etc. The divertor heat load is evaluated by using simplified scaling models. There are two reasons for this simple approach. First, the detailed local transport in the core plasma and divertor region has not well been understood. Second, the more sophisticated 2-D calculation is much more time consuming and is not suitable for the parametric study. Three types of divertor scaling models are compared.

In Chap. 2, we give a brief description of TPC code used to

analyze the operation points of ITER. The calculation models of divertor heat load are also described there. In Chap. 3, we concentrate on steady-state mode operations. Steady-state operation region of ITER is reviewed and the divertor heat load is predicted by using several scaling models. Operation points are optimized with respect to divertor heat load and requirements to reduce the heat load down to the level of ignition mode are discussed. Several methods to improve the divertor condition are also investigated. In Chap. 4, we investigate the hybrid mode operations. The operation points are optimized under the condition where the burn time is longer than 2000 s, which is necessary for the technology testing. Relation between the controllability of plasma current-profile and the divertor heat load is also discussed. Chapter 5 gives the conclusions and summary.

2. TPC Code

2-1 Power Balance Calculation

In this section, assumptions used in the analyses are described briefly. At thermal equilibrium, the plasma heating powers are balanced against the plasma power losses. That is,

$$P_{\alpha} + P_{OH} + P_{NBI} = \frac{W_P}{\tau_E} + P_{BR} + P_{SYN} + P_{LIN},$$

where P_{α} is alpha heating power, P_{OH} is ohmic power, P_{NBI} is auxiliary heating power, W_P is stored energy, τ_E is the energy confinement time, P_{BR} is bremsstrahlung loss power, P_{SYN} is synchrotron loss power and P_{LIN} is line radiation losses, respectively. In this report, we consider only neutral beam injection (NBI) heating for simplicity. Carbon (C), oxygen (O) and iron (Fe) are assumed as impurities. Fractions of C and Fe to the electron density (n_e) depend on n_e. Fraction of O is fixed to 0.1 %.

analyze the operation points of ITER. The calculation models of divertor heat load are also described there. In Chap. 3, we concentrate on steady-state mode operations. Steady-state operation region of ITER is reviewed and the divertor heat load is predicted by using several scaling models. Operation points are optimized with respect to divertor heat load and requirements to reduce the heat load down to the level of ignition mode are discussed. Several methods to improve the divertor condition are also investigated. In Chap. 4, we investigate the hybrid mode operations. The operation points are optimized under the condition where the burn time is longer than 2000 s, which is necessary for the technology testing. Relation between the controllability of plasma current-profile and the divertor heat load is also discussed. Chapter 5 gives the conclusions and summary.

2. TPC Code

2-1 Power Balance Calculation

In this section, assumptions used in the analyses are described briefly. At thermal equilibrium, the plasma heating powers are balanced against the plasma power losses. That is,

$$P_\alpha + P_{OH} + P_{NBI} = \frac{W_P}{\tau_E} + P_{BR} + P_{SYN} + P_{LIN},$$

where P_α is alpha heating power, P_{OH} is ohmic power, P_{NBI} is auxiliary heating power, W_P is stored energy, τ_E is the energy confinement time, P_{BR} is bremsstrahlung loss power, P_{SYN} is synchrotron loss power and P_{LIN} is line radiation losses, respectively. In this report, we consider only neutral beam injection (NBI) heating for simplicity. Carbon (C), oxygen (O) and iron (Fe) are assumed as impurities. Fractions of C and Fe to the electron density (n_e) depend on n_e. Fraction of O is fixed to 0.1 %.

Therefore, the effective ion charge (Z_{eff}) also depends on n_e. Helium accumulation for the typical case is assumed to be 10 %. Typical values of Z_{eff} are 1.7 at $n_e=1.2\times10^{20}m^{-3}$ and 2.2 at $n_e=0.6\times10^{20}m^{-3}$. It is assumed that the wall reflectivity for the synchrotron loss is 80 %. Radiation losses from the plasma are calculated according to ITER Physics design guidelines [3].

Required energy confinement time is compared with ITER-89 L-mode scaling laws and the confinement enhancement factor (H-factor) is evaluated. Generally, confinement time evaluated by the scaling law is a function of net heating power P_{HEAT}. We do not subtract the synchrotron loss power from P_{HEAT}. That is,

$$P_{HEAT} = P_{\alpha} + P_{OH} + P_{NBI} - (P_{BR} + P_{LIN}) .$$

This assumption is conservative since the estimation of H-factor is larger than the case that P_{SYN} is subtracted.

The current-drive efficiency of NBI is based on ITER physics design guidelines [3]. Bootstrap current I_{BS} is calculated by the following equations [4];

$$I_{BS} / I_P = C_{BS} (\varepsilon^{0.5} \beta_p)^{1.3},$$

$$C_{BS} = 1.32 - 0.235(q_{\Psi}/q_0) + 0.0185(q_{\Psi}/q_0)^2,$$

where I_P is the plasma current, ε is the inverse aspect ratio, β_p is poloidal beta value, q_{Ψ} is MHD safety factor at 95 % magnetic surface and q_0 is the safety factor at the axis, respectively.

Major radius (R_p) is 6.0 m, minor radius (a_p) is 2.15 m, elongation (κ) is 2.0 and triangularity (δ) is 0.35, respectively. Table 1 lists the major plasma parameters and machine parameters of ITER. Reference operation points of ITER calculated by TPC code are shown in Table 2. In this report, we designate the specific operation points as I_n, S_n and H_n (n=1,2,3...). Here I, S and H denote ignition, steady-state and hybrid mode, respectively. And we also designate general operation points, such as the lowest-I_P point, by Point A, Point B, etc.

2-2 Calculation of Divertor Heat Load

In this section, we review the model of the divertor heat load briefly and introduce several scaling models. The peak divertor heat load W_{div} (MW/m^2) is described by

$$W_{div} = \frac{f_{div} \cdot P_{div}}{2\pi R_{div}} \cdot \frac{1}{\Delta_P} \cdot \sin\Theta ,$$

where P_{div} (MW) is the power inflow to the divertor region and given by

$$P_{div} = P_{\alpha} + P_{OH} + P_{NBI} - (P_{BR} + P_{SYN} + P_{LIN} + P_{EDGE}).$$

Here, P_{EDGE} is the radiation loss in SOL region. $1/\Delta_P$ (m^{-1}) is the peaking factor of the heat flux, that is an inverse of the half width of heat flux. R_{div} is the position of striking point and Θ is the angle between the separatrix field line and the divertor plate in the poloidal cross-section, respectively. And f_{div} is the fraction of the power to the plate considered, that is, f_{div}= 0.6 for the outer plate of SN divertor, 0.4 for the inner plate of SN divertor and the outer plate of DN divertor and 0.1 for the inner plate of DN divertor.

According to the experiments in JT-60U [5], $1/\Delta_P$ is found to be proportional to $Q_{div}^{0.49} n_e^{-0.46} q_{eff}^{-0.67}$ (See Fig. 1). Here, q_{eff} is the effective q value, $Q_{div} = P_{div} / S_P$ and S_P is the plasma surface area. Therefore, we obtain the following scaling model;

$$W_{div}^{JT\text{-}60U} \propto P_{div}^{1.49} n_e^{-0.46} I_P^{0.67}. \qquad \text{[JT-60U model]}$$

Theoretical scaling models are also proposed [6,7]. By using the equation of thermal conduction perpendicular to the magnetic field line, $1/\Delta_P$ is scaled as follows;

$$\frac{1}{\Delta_P} \propto Q_{div}^{5/9} n_S^{-7/9} \chi_{\perp}^{-7/9} L^{-4/9},$$

where n_s is the electron density at the mid-plane separatrix, $\chi_\perp$ is the transverse thermal diffusion coefficient and L (= $R_P q_\Psi$) is the connection length, respectively. In this report, we will use two typical models for $\chi_\perp$. The first one is that $\chi_\perp$ is constant. In this case, we have

$$W_{div}^{Const\text{-}\chi} \propto P_{div}^{14/9}\, n_e^{-7/9}\, I_P^{4/9} . \qquad \text{[Const-}\chi\text{ model]}$$

Here, we assume n_s is proportional to n_e [8]. Another typical case is the Bohm diffusion case. In this case, by using $\chi_\perp \propto P_{div}^{3/4} / n_e^{1/2}$, we obtain

$$W_{div}^{Bohm\text{-}\chi} \propto P_{div}\, n_e^{-0.4}\, I_P^{4/9} . \qquad \text{[Bohm-}\chi\text{ model]}$$

In ITER CDA, Const-χ model (Harrison-Kukushkin's simplified model [6]) is adopted to estimate the divertor heat load together with 2-D calculations [8]. In the following part of this report, we use above mentioned three models to evaluate the divertor heat load. Note that W_{div} is a function only of P_{div}, n_e and I_P for the specific machine. W_{div} is normalized to 5 MW/m^2 at the ITER reference ignition point (I_1) where P_{div} = 116 MW, n_e = 1.22×10^{20} m^{-3} and I_P = 22 MA.

3. Optimization of Steady-state Mode Operation

3-1 Steady-state Operation Region

In this section, we review a steady-state operation of ITER. Optimization of the operation points is done in the next section. Major restrictions for the steady-state operation are beta limit, energy confinement time and available current-drive power.

The maximum value of the toroidal beta β_t is proportional to the plasma current I_P. That is,

where n_s is the electron density at the mid-plane separatrix, $\chi_\perp$ is the transverse thermal diffusion coefficient and L (= $R_P q_\Psi$) is the connection length, respectively. In this report, we will use two typical models for $\chi_\perp$. The first one is that $\chi_\perp$ is constant. In this case, we have

$$W_{div}^{Const\text{-}\chi} \propto P_{div}^{14/9}\, n_e^{-7/9}\, I_P^{4/9} . \qquad \text{[Const-}\chi\text{ model]}$$

Here, we assume n_s is proportional to n_e [8]. Another typical case is the Bohm diffusion case. In this case, by using $\chi_\perp \propto P_{div}^{3/4} / n_e^{1/2}$, we obtain

$$W_{div}^{Bohm\text{-}\chi} \propto P_{div}\, n_e^{-0.4}\, I_P^{4/9} . \qquad \text{[Bohm-}\chi\text{ model]}$$

In ITER CDA, Const-χ model (Harrison-Kukushkin's simplified model [6]) is adopted to estimate the divertor heat load together with 2-D calculations [8]. In the following part of this report, we use above mentioned three models to evaluate the divertor heat load. Note that W_{div} is a function only of P_{div}, n_e and I_P for the specific machine. W_{div} is normalized to 5 MW/m^2 at the ITER reference ignition point (I_1) where P_{div} = 116 MW, n_e = 1.22×10^{20} m^{-3} and I_P = 22 MA.

3. Optimization of Steady-state Mode Operation

3-1 Steady-state Operation Region

In this section, we review a steady-state operation of ITER. Optimization of the operation points is done in the next section. Major restrictions for the steady-state operation are beta limit, energy confinement time and available current-drive power.

The maximum value of the toroidal beta β_t is proportional to the plasma current I_P. That is,

$$\beta_t\,(\%) = g\cdot\frac{I_P\,[MA]}{a_P\,[m]\;B_T\,[T]} \qquad (\,g < g_{cr}\,),$$

where a_P is the plasma minor radius and B_T is the toroidal magnetic field, respectively. The value of the proportionality constant (g) is called Troyon coefficient and must be smaller than the critical value (g_{cr}). Here, $g_{cr} = 2 \sim 5$ depending on the plasma shape, the current profile, etc. In case of a steady-state plasma, we assume that $g_{cr} = 3.0$ because the current-profile control might be possible, while $g_{cr} = 2.0$ is adopted for the ignition mode of ITER. It is not clear at present whether only the perpendicular component of the injected beam pressure should be included in β-limit or whether the entire beam pressure should contribute. In this report, we assume that all component of the beam beta β_b contribute to β_t. This assumption is more conservative than the case that one third of β_b is included [1].

Confinement constraints are expressed in terms of the maximum permissible enhancement (H-factor) over L-mode energy confinement scaling laws. In this report, we consider two types of scaling laws, i.e., ITER-89 power scaling law and ITER-89 offset-linear scaling law. For these scaling laws, the confinement time increases with I_P. Typical value of H-factor in the present experiments of large tokamaks is smaller than 2. H-mode experiments in JET and ASDEX show that H-factor for ITER-89 power scaling law is sometimes about 2.2 [1]. In this chapter, we assume that the maximum value of H-factor is 2.1 following the previous work [1,2].

Another constraint is the available current-drive power P_{NBI}. Since the current-drive efficiency is approximately proportional to the electron temperature T_e, the required power is larger in lower-T_e region (and naturally in higher-I_P region). In this report, we assume that the maximum value of P_{NBI} is 120 MW.

Fusion gain, or energy multiplication, Q may be another key issue. It is because the steady-state operation with $Q > 5$ might be necessary to extrapolate to DEMO reactor. In the previous work [1,2], the condition $Q \geq 5$ is used instead of $P_{NBI} \leq 120$ MW. Obviously, the latter is stricter than the former when the fusion

power P_{FUS} > 600 MW, which is the region of our concern. Therefore, we adopt the latter condition in this report.

For the reasons mentioned above, it is convenient to express the operation region of a steady-state plasma in T_e- I_P space together with the contour lines of g, H-factor and P_{NBI}. Next, we show the steady-state operation region by using above mentioned two scaling laws.

(i) ITER-89 power scaling law

Figure 2 shows the steady-state operation region for various fusion powers P_{FUS}. H-factor is evaluated by using ITER-89 power scaling law. Average neutron wall load L_{WAL} is also shown in the figures. In all figures, solid lines, dashed lines and short-long dashed lines denote contour lines of H-factor, P_{NBI} and Troyon g, respectively. Note that the loop voltage V_{LOOP} is equal to 0 V everywhere and the fusion gain Q is not constant on this T_e-I_P plane. The MHD safety factor q_ψ > 3 is another constraint. Here, q_ψ = 3 is corresponding to I_p = 22 MA. Therefore, operation is possible in the shaded area of the figures. It is seen that the operation region is limited mainly by the confinement capability (H-factor) not by the beta limit (Troyon g) when the fusion power P_{FUS} is relatively small. It is also seen that the possible operation area becomes very small when the average neutron wall load L_{WAL} goes up to 0.6 MW/m^2, corresponding to about 1 MW/m^2 in the testing region, which is considered to be the minimum requirement for the technology testing. It is also seen that there is no steady-state operation region when P_{FUS} is larger than about 750 MW, since Troyon g exceeds the critical value. The reference operation point for steady-state mode is also shown on Fig.2-c) by Point S_1. The reason why this point is chosen is explained in the next section.

When the condition H ≤ 2.0 is adopted instead of the condition H ≤ 2.1, the maximum fusion power goes down to about 690 MW. The operation point with the lowest-I_P for this case is shown in Fig.2-b) by Point S_2.

(ii) ITER-89 offset-linear scaling law

Figure 3 shows the steady-state operation region for various fusion powers P_{FUS} when H-factor is evaluated by using ITER-89 offset-linear scaling law. In this case, the operation point is limited mainly by Troyon g rather than H-factor. Therefore, the lowest value of I_P increases with P_{FUS}. If the restriction on Troyon coefficient g is removed, the operation is limited by H-factor and the lowest value of I_P does not change much when P_{FUS} increases. Note that no restriction appears on P_{FUS} when H-factor is calculated by this scaling law, while the maximum value of P_{FUS} is about 1000 MW for the power scaling law.

3-2 Divertor Heat Load for Steady-state Operation

The scaling model of divertor heat load considered in this report is generally written as follows;

$$W_{div} \propto (P_{\alpha} - P_{RAD} + P_{NBI})^{a} I_P^{b} / n_e^{c} \qquad (a, b, c > 0),$$

where P_{RAD} is the total radiation loss power. Then, the divertor heat load increases as I_P becomes large and decreases as n_e becomes high. On the other hand, n_e becomes high as T_e decreases when the fusion power is fixed. In case of steady-state operations, however, the lower-T_e requires the larger-P_{NBI} due to the low efficiency of current-drive. Therefore, the first term of the above equation becomes large. The resultant value of the divertor heat load depends on the exponent of each term.

Figure 4 shows the steady-state operation region for ITER-89 power scaling law when P_{FUS} = 450 MW. This figure is corresponding to Fig. 2-a). Point A represents the operation point for the largest-P_{NBI}, the smallest-T_e and the smallest-I_P. Point B denotes the operation point for the smallest-P_{NBI}, the highest-T_e and the highest-I_P. Point C represents the operation point for the

largest-P_{NBI}, the smallest-H and the highest-I_p. The divertor heat load and other plasma parameters at these points are shown in Table 3. It is seen that the divertor heat load at Point A is the smallest for all scaling models. The result does not change even when ITER-89 offset-linear scaling law is used.

Practically, the current-drive power should be at least 5~10 % smaller than the maximum value available. Figure 5 shows the divertor heat load and the required current-drive power when the operation point moves from A to B on the contour line of H = 2.1 in Fig. 2-c). It is seen that the divertor heat load does not increase very much when the operation point moves from A to B and the beam power takes the minimum value at Point S_1. Hence the ITER reference point of steady-state mode is selected as the one shown in Table 2.

In this report, we investigate the minimum divertor heat load. Therefore, we adopt the lowest-I_p point (Point A) as the optimized point for this fusion power. Note that the dependence on the plasma current I_p is dominant in these cases, since $(I_p{}^A/I_p{}^B)^{4/9} \sim 0.8$. This implies that the dependence of the divertor heat load on the plasma current I_p or the connection length L ($=R_p q_\Psi$) is important for this kind of analysis.

3-3 Divertor Heat Load for Various Fusion Powers

(i) ITER-89 power scaling law

Figure 6 shows the divertor heat load at the lowest I_p point (Point A) for various fusion powers. Here, ITER-89 power scaling law is assumed. It is seen that the dependence of the divertor heat load on the fusion power is similar for all models considered. When P_{FUS} = 750 MW, the heat load given by Const-χ model is 1.8 times larger than that given by Bohm-χ model. The heat load given by JT-60U model takes the intermediate value.

(ii) ITER-89 offset-linear scaling law

Figure 7 shows the divertor heat load at Point A for various fusion powers in case of ITER-89 offset-linear scaling law. The dependence of the heat load on the fusion power is similar to that of ITER-89 power scaling law. When P_{FUS} = 750 MW, the heat load values are about equal to those for power scaling law. When P_{FUS} < 750 MW, the heat load is smaller in offset-linear scaling law than in power scaling law.

Figure 8 shows the possible highest fusion power as a function of the allowable divertor heat load for several divertor models. This figure is the case for ITER-89 power scaling law. It is seen that the possible highest fusion power much differs for each model when the allowable divertor heat load is given. Therefore, it should be important to refine the divertor scaling model in the future physics R & D. The possible fusion power is 200 ~ 400 MW when the maximum allowable heat load is 5 MW/m^2. This value may be too small for the technology testing.

3-4 Reduction Scheme of Divertor Heat Load

In the previous section, we investigate the achievable fusion power under the conditions given by the ITER guidelines. In this section, we discuss the several reduction methods of the divertor heat load by improving the helium accumulation, the confinement capability and the current-drive efficiency when P_{FUS} = 690 MW as an example. We also give the target of physics R & D.

In case of ITER-89 offset-linear scaling law, it is seen from Fig.3 that the very low operation temperature (consequently high operation density) can be chosen if the constraint on Troyon g is removed. Therefore, it is an important physics R & D to achieve high-g operation when this scaling law holds. In fact, the divertor heat load for the steady-state mode operation can be reduced to the level of ignition mode (~ 5 MW/m^2) if Troyon g can be

increased up to 3.6 (Point S_0 in Table 4). In the following part, only ITER-89 power scaling law is used to estimate the H-factor since this scaling law gives stricter constraint for the operation region than ITER-89 offset-linear scaling law.

Figure 9 shows the minimum divertor heat load as a function of helium concentration when P_{NBI} = 120 MW, H = 2 and g ≤ 3. It is seen that the heat load decreases by about 15 % for all models as the helium concentration is reduced from 10 % to 6 %. This reduction is attributed to the decrease of the plasma current due to the decrease of the fuel dilution effect, which leads to the decrease of the operation temperature and increase of the density to achieve the same fusion power.

Figure 10 shows the minimum divertor heat load as a function of H-factor when P_{NBI} = 120 MW and g ≤ 3. Here, the helium concentration is fixed to 10 %. It is seen that the heat load decreases by 20 ~ 25 % for all models as H-factor increases from 2.0 to 2.2. It is because the plasma current at the operation point becomes low due to the good confinement, which is basically the same as the case with decreasing helium concentration.

Figure 11 shows the minimum divertor heat load as a function of the current-drive efficiency γ normalized by γ_{ITER} when P_{NBI} = 120 MW, H = 2 and g ≤ 3. Here, γ_{ITER} is the current-drive efficiency given by the ITER guidelines. It is seen that the heat load decreases by 20 ~ 30 % as γ/γ_{ITER} increases from 1.0 to 1.4. It is because the operation temperature becomes low due to the good current-drive efficiency.

It is considered that the additional impurity seeding is effective because the radiation loss becomes large [1,2]. Figure 12 shows the minimum divertor heat load as a function of the concentration of Fe when H = 2.1, g ≤ 3 and P_{FUS} = 750 MW. In this case, the required P_{NBI} increases due to the increase of the radiation loss. Corresponding Z_{eff} and P_{NBI} are shown in Fig. 13. Nevertheless, it is seen that the heat load decreases drastically for all models as Fe concentration increases. The heat load decreases to the level of ignition mode of operation (about 5 ~ 6 MW/m^2) when Fe concentration increases from 0.06 % to 0.28 %. In this case, however, P_{NBI} increases from 120 to 150 MW and Z_{eff}

increases from 2.2 to 3.5. Further study should be done experimentally since the effect of impurity seeding on the confinement of the main plasma is unknown.

Figure 14 shows the synergetic effect of the above mentioned improvements. Operation point S_4 in the figure is the most optimistic case of the present study, where H = 2.5 and the improvement in current-drive efficiency of 40 % are assumed. Here, P_{FUS} = 690 MW and He accumulation is assumed to be 5 %. Reference operation point S_3 with the lowest-I_P for P_{FUS} = 690 MW is also shown in the figure. The divertor heat load at Point S_4 is about 5 ~ 6 MW/m^2, which is the level of the ITER reference ignition point. On the other hand, the H-factor given by ITER-89 offset-linear scaling law is about 1.78 at Point S_4. The plasma parameters at Point S_3 and Point S_4 are listed in Table 4.

4. Optimization of Hybrid Mode Operation

4-1 Requirement for Hybrid Mode

As is discussed in the previous chapter, a steady-state mode operation with high wall load (L_{wal} > 0.6 MW/m^2) requires a large improvement of the plasma performance. In the hybrid mode operations, both non-inductive and inductive current-drive are employed. Therefore, an operation point with the higher density can be chosen, since the required driven current is smaller than that of the steady-state operations. This fact tends to relieve the divertor condition. Hence, this mode could be the best operation mode for the technology phase of ITER.

The penalty incurred with the hybrid operation is the finite burn time. Therefore, we must determine the minimum burn time to optimize the operation parameters. The minimum burn time required should be determined by the mission of experiments and the time scales of the phenomena concerned. The time scales are divided into next two groups;

increases from 2.2 to 3.5. Further study should be done experimentally since the effect of impurity seeding on the confinement of the main plasma is unknown.

Figure 14 shows the synergetic effect of the above mentioned improvements. Operation point S_4 in the figure is the most optimistic case of the present study, where H = 2.5 and the improvement in current-drive efficiency of 40 % are assumed. Here, P_{FUS} = 690 MW and He accumulation is assumed to be 5 %. Reference operation point S_3 with the lowest-I_P for P_{FUS} = 690 MW is also shown in the figure. The divertor heat load at Point S_4 is about 5 ~ 6 MW/m^2, which is the level of the ITER reference ignition point. On the other hand, the H-factor given by ITER-89 offset-linear scaling law is about 1.78 at Point S_4. The plasma parameters at Point S_3 and Point S_4 are listed in Table 4.

4. Optimization of Hybrid Mode Operation

4-1 Requirement for Hybrid Mode

As is discussed in the previous chapter, a steady-state mode operation with high wall load (L_{wal} > 0.6 MW/m^2) requires a large improvement of the plasma performance. In the hybrid mode operations, both non-inductive and inductive current-drive are employed. Therefore, an operation point with the higher density can be chosen, since the required driven current is smaller than that of the steady-state operations. This fact tends to relieve the divertor condition. Hence, this mode could be the best operation mode for the technology phase of ITER.

The penalty incurred with the hybrid operation is the finite burn time. Therefore, we must determine the minimum burn time to optimize the operation parameters. The minimum burn time required should be determined by the mission of experiments and the time scales of the phenomena concerned. The time scales are divided into next two groups;

1) Physics issues:

Time scales of thermal instability, particle confinement and α-heating are several seconds to several tens of seconds. Helium ash exhaust experiment will require 100 s of pulse duration time. The longest time scale in this category would be the resistive skin time, which is about several hundred to several thousand seconds. At least 1000 s of the pulse length would be required for the current-profile control experiment.

2) Technology issues:

Thermal response of the reactor components should be tested in ITER technology phase. Thermal response of divertor plates is less than 10 s. Response of the first wall is considered to be 100 ~1000 s. Response of the blanket test module is more than 1000 s.

Another important issue is the required total neutron fluence for the technology testing. The required neutron fluence at the test module is about 1 MWa/m^2. It means that the required total operation period is at least 3.2×10^7 s when the peak neutron wall load is 1 MW/m^2. On the other hand, the maximum number of operations is considered to be 40000 shots by the fatigue problem of the components, e.g., center solenoid coils. Therefore, 1000 s is the minimum requirement for the pulse duration time to this matter.

In this report, we assume that the minimum requirement for the burn time is 2000 s. We also assume that the minimum value of the average neutron wall load L_{wal} is 0.6 MW/m^2 (P_{FUS} = 690 MW) since the local neutron wall load near the mid-plane will be about 1.6 times larger than the average value. The maximum value of Troyon g is assumed to be 3.0 same as steady-state operations. The maximum value of H-factor is assumed to be 2.0 for typical cases. Note that operation point generally exists anyway for all values of H-factor unlike the steady-state mode operations.

4-2 Calculation of Burn Time

In this section, we estimate the magnetic flux consumption and calculate the burn time T_{burn} of ITER. In order to calculate the burn time, we have to know the supplied flux. Total flux supplied by PF coil system consists of two parts, the flux Φ_{OH} supplied by the center solenoid (CS) coil and the flux Φ_{VF} given by the vertical field (VF) coil. That is,

$$\Phi_{total} = 2 \times \Phi_{OH} + \Phi_{VF},$$

where

$$\Phi_{OH} = \pi R_{OH}^2 B_{PMAX} f_{OH},$$

$$\Phi_{VF} = \pi R_p^2 B_V f_{VF},$$

and R_{OH} is the radius of CS coil, B_{PMAX} is the maximum magnetic field of CS coil and B_V is Shafranov vertical field, respectively. Here, f_{OH} (~ 1.04) is a factor due to the finite dimension of CS coil and f_{VF} (~ 0.65) is the factor that is obtained by the equilibrium calculation for the typical case. Note that Φ_{VF} is approximately proportional to the plasma current I_P.

Once the loop voltage V_{loop} is determined, T_{burn} is calculated by the relation $T_{burn} = \Phi_{burn}/V_{loop}$. Here Φ_{burn} is the flux available for the flat top and given by

$$\Phi_{burn} = \Phi_{total} - \Phi_{heat} - \Phi_{ramp},$$

where Φ_{heat} (=10 Vs) is the flux used during heating phase and Φ_{ramp} is the flux which is necessary for the current ramp-up and estimated by

$$\Phi_{ramp} = (L_P + 0.4 \mu_0 R_P) I_P.$$

Here, μ_0 is the vacuum permeability and L_P is the self-inductance of the plasma. In the following part, we estimate the burn time by

using these relations. Coil design parameters are listed in Table 1. Typical values of the magnetic flux for ITER reference points are shown in Table 2.

4-3 Achievable Burn Time and Divertor Heat Load

In this section, we estimate the achievable burn time when the fusion power and the current-drive power are given. The T_e-I_P space analysis can also be used to investigate long burn (hybrid mode) operations systematically same as steady-state cases.

Figure 15 shows an example of the operation space for hybrid mode when P_{FUS} = 860 MW and P_{NBI} = 80 MW. Note that Q = 10.7 everywhere and V_{loop} is not constant in T_e-I_P space for this case. H-factor (dashed line) is calculated by using ITER-89 power scaling law. The upper part of the dashed line is the region where $H \leq 2$. The reason why H-factor takes the minimum value around T_e=10 keV for the same I_P is that the ratio of W_P to $P_\alpha^{1/2}$ also takes the minimum value at this temperature, which comes from the temperature dependence of the fusion cross-section [2]. Contour lines of burn time are also shown by solid lines. Steady-state region appears at the lower right-hand corner of the figure. It is seen that the longest burn time is achieved when T_e = 15.5 keV and I_P = 19 MA for $H \leq 2.0$ (Point A in Fig. 15). Point A is called the point with the achievable (longest) burn time in this report. The burn time T_{burn} is about 2700 s at this point. Point B is the operation point where H = 2.0 and $g \leq 3.0$ and the burn time is 2000 s. Similar graphs can be drawn and the longest burn time can be obtained for any P_{FUS} and P_{NBI}. Results are shown in Fig. 16, which shows the contour lines of the achievable longest burn time in P_{FUS}-P_{NBI} space. Point S_1 shows the ITER reference operation point of steady-state mode. Point I_1 denotes the reference point of ignition mode and Point H_1 the reference point of hybrid mode.

It is seen that NBI power should be larger than about 60 MW in order to obtain the burn time longer than 2000 s that is

required for the technology testing. We assume that the minimum requirement for the fusion power is 690 MW in this report. Troyon g exceeds the critical value at the upper right-hand corner. Therefore, the operation region is inside of the hatched triangle. The reason why Troyon g increases with P_{NBI} is that the plasma current at the longest burn time decreases.

Figure 17 shows the divertor heat load W_{div} at the longest burn time for Const-χ model corresponding to Fig. 16. Figures 18 and 19 show the contour lines of W_{div} for Bohm-χ model and for JT-60U empirical scaling model, respectively. It is seen that W_{div} is larger in larger-P_{FUS} and larger-P_{NBI} region for all models. Therefore, the divertor heat load is minimum when both P_{NBI} and P_{FUS} are minimum (Point H_2). The heat load at Point H_2 is about 9 MW/m^2 for Const-χ model, about 7 MW/m^2 for Bohm-χ model and about 8 MW/m^2 for JT-60U model.

The reason why the divertor heat load at Point I_1 is larger than 5 MW/m^2 is that the operation temperature is higher than 10 keV and the burn time is longer than 400 s. The plasma parameters at Point H_2 are shown in Table 5.

4-4 Reduction Scheme of Divertor Heat Load

In this section, we optimize the operation point with respect to the burn time. We assume that the required burn time for technology testing is 2000 s. The divertor heat load can be reduced by decreasing the burn time down to 2000 s when the achievable burn time is longer than 2000 s. In Fig.15, for example, the burn time decreases as the operation point moves from Point A to Point B on the contour line of H = 2.0 and the operation temperature is reduced with the decrease of the burn time.

Figure 20 shows the burn time at Points A and B as a function of P_{NBI} when H = 2.0 and P_{FUS} = 860 MW. It is seen that the achievable burn time is prolonged as P_{NBI} increases and the operation reaches steady-state when P_{NBI} is about 120 MW.

Figure 21 shows the corresponding divertor heat load W_{div}

(Const-χ model). Closed circles denote W_{div} at the achievable longest burn time and open circles denote W_{div} at the burn time of 2000 s. It is seen that W_{div} at the burn time of 2000 s (B) decreases as P_{NBI} increases, while W_{div} at the longest burn time (A) increases with P_{NBI}. Similar tendency is shown for all models (See Figs. 22 and 23).

The contour lines of W_{div} for hybrid operations with burn time of 2000 s are shown in Fig. 24. Here, H = 2.0 and Const-χ model is used. It is seen that the divertor heat load W_{div} becomes larger as the fusion power increases. The tendency is similar for all models (See Figs. 25 and 26). Therefore, we can conclude that the divertor heat load takes the minimum value when P_{NBI} takes the installed maximum value and P_{FUS} takes the allowable minimum value for the technology testing.

When the maximum value of P_{NBI} is 110 MW and the minimum value of P_{FUS} is 690 MW, the minimum value of the heat load is achieved at Point H_3, the value of which is 7.3 MW/m^2 for Const-χ model, 6.0 MW/m^2 for Bohm-χ model and 6.4 MW/m^2 for JT-60U model.

If we can expect the further enhancement of H-factor, the divertor heat load can be reduced still more. The divertor heat load at Point H_3 can be reduced down to the level of the ignition mode without impurity seeding by increasing H-factor up to 2.2, which is the value used in the reference point (H_1). The burn time, however, is 2000 s, while it is 2500 s at Point H_1. The parameters for this case are listed as Point H_4 in Table 5.

Divertor heat load at Point H_1 can be also reduced to the level of the ignition mode without impurity seeding by reducing the burn time from 2500 s to 2000 s (Shown by Point H_5 in Table 5). However, H-factor should be increased up to 2.3 to secure the burn time of 2500 s without impurity seeding (Point H_6). The parameters of these points are also listed in Table 5.

It is seen from Figs. 24, 25 and 26 that the divertor heat load decreases 10 ~ 20 % by increasing the beam power from 70 MW to 90 MW, but the heat load changes little beyond that. Therefore, the best operation point may be at the intermediate area between

H_2 and H_3. The choice of operation points must be judged by considering the controllability for the current profile.

The operation points obtained in this section satisfy the requirements mentioned in Sec. 4-1. The ratio of the beam-driven current to the plasma current for these points, however, is smaller than that for Point H_1 or H_2. This fact may lead to some disadvantage since this ratio is related to the controllability of the current-profile. This issue is discussed in the next section.

4-5 Controllability and Divertor Heat Load

The current-profile controllability is also an important issue. In a steady-state mode operation, the plasma is operated at a rather limited operation space near the beta limit to satisfy various constraints. Therefore, the plasma will need a specific range of current profiles. ITER guidelines require that more than 30 % of the plasma current is to be driven non-inductively to retain adequate current-profile control. In this report, we define the controllability by I_{NBI}/I_P. Here, I_{NBI} is the beam driven current. In case of steady-state mode, it is not difficult to satisfy the condition. Actually all steady-state operation points obtained in Chap. 3 satisfy the condition. For the hybrid mode operations, this condition is critical as is shown below.

In this section, we estimate the upper limit of the achievable controllability and investigate the relation between the controllability and the divertor heat load. According to the definition of toroidal beta β_t, we have

$$\beta_t = 2\times10^{25}\mu_0 k_B(1+f_b)\ (1+f_{ie})\ n_{20}\ T_e\ [\mathrm{keV}]\ /\ B_T{}^2 \qquad (\%),$$

where k_B is Boltzmann constant ($\sim 1.602\times10^{-19}$), $f_b=(\beta_b+\beta_\alpha)/\beta_{th}$, $f_{ie}=n_i/n_e$ and $n_{20}=n_e/10^{20}$ m^{-3}, respectively. Here, β_b, β_α and β_{th} denote the beam component, alpha component and the thermal component of the toroidal beta. By using Troyon coefficient g, the

above equation can be expressed by

$$T_e\ [\mathrm{keV}] = 0.2484\ \frac{B_T}{a_p(1+f_b)\ (1+f_{ie})}\ g\ I_P\ [\mathrm{MA}]\ /\ n_{20}.$$

On the other hand, the current-drive efficiency η_{NBI} is approximately given by

$$\eta_{NBI} = 0.0039\ T_e\ [\mathrm{keV}]\ /\ n_{20} \qquad [\mathrm{A/W}].$$

Then we finally obtain a formula for the controllability as follows;

$$I_{NBI}\ /\ I_P = C_{NBI}\ P_{NBI}\ [\mathrm{MW}]\ g\ /\ n_{20}^{\,2} \qquad (\%),$$

where

$$C_{NBI} = 0.0484\ \frac{B_T}{a_p(1+f_b)\ (1+f_{ie})/2}.$$

For typical cases, $(1+f_{ie})/2 = 0.89 \sim 0.95$ and $1+f_b = 1.1 \sim 1.2$. Then we have $C_{NBI} = 0.09 \sim 0.11$. Generally the larger P_{NBI} is, the smaller C_{NBI} is. Therefore, we can conclude that the upper limit of the controllability is estimated by $I_{NBI}/I_P \leq 30/n_{20}^{\,2}$ %, when $P_{NBI} \leq$ 110 MW and $g \leq 3$. This estimation implies that the electron density should be smaller than 1×10^{20} m^{-3} in order to secure the controllability more than 30 %. Steady-state operation points satisfy this condition (Note that $g > 3$ for S_4 and S_0).

On the other hand, the most optimistic divertor scaling model considered in this report is

$$W_{div}^{\text{Bohm-}\chi} = 0.0118\ \ P_{div}\ I_P^{4/9}/\ n_{20}^{0.4} \qquad [\mathrm{MW/m^2}].$$

Here, the units of P_{div} and I_P are MW and MA, respectively. Figures 27 and 28 show the contour line plots of P_{div} at the operation point of the longest burn time and of 2000 s burn time, respectively. It is seen that the smallest P_{div} without impurity seeding is about 140 MW when $P_{FUS} \geq 690$ MW and $T_{burn} \geq 2000$ s.

The reason why P_{div} at the operation point of 2000 s is smaller than that at the operation point of the longest burn time is the enhanced radiation power due to the higher density (the lower temperature for the same fusion power). The achievable lowest-I_P is about 14 MA when $P_{FUS} \geq 690$ MW and $P_{NBI} \leq 120$ MW (See Fig. 29). Then, we obtain $W_{div} > 5.3 / n_{20}^{0.4}$ MW/m^2, which means that n_e should be larger than 1×10^{20} m^{-3} in order to reduce the divertor heat load down to the level of ignition mode (5 MW/m^2). For this reason, the low divertor heat load (< 5 MW/m^2) is hardly compatible with the high controllability (>30 %). Figures 30 and 31 show the contour line plots of the controllability (I_{NBI}/I_P) at the operation point of the longest burn time and of 2000 s burn time, respectively. It is seen that I_{NBI}/I_P decreases from 63 % to 23 % at Point H_3 when the operation point is optimized by reducing the burn time. On the other hand, the divertor heat load decreases from 14.8 MW/m^2 to 7.3 MW/m^2 (Const-χ case) to make up for it. The best operation point is Point H_2, if the controllability must be larger than 30 %.

The controllability (I_{NBI}/I_P) of Point H_4 obtained in the previous section is 18 %. MHD safety factor at Point H_4 (4.8) is a little larger than that of Point H_1 (4.3) and Troyon g is smaller than the maximum value (3.0). These facts may lead to the relaxation of the requirement of controllability somewhat. It should be an important physics R & D how much controllability is required.

5. Conclusions and Summary

(i) Steady-state mode operations

Steady-state mode operations of ITER are investigated. There is an operation window when the fusion power P_{FUS} is less than about 750 MW. Here, we assume that $P_{NBI} \leq 120$ MW, Troyon g ≤ 3 and H ≤ 2.1. The maximum fusion power decreases down to about

The reason why P_{div} at the operation point of 2000 s is smaller than that at the operation point of the longest burn time is the enhanced radiation power due to the higher density (the lower temperature for the same fusion power). The achievable lowest-I_P is about 14 MA when $P_{FUS} \geq 690$ MW and $P_{NBI} \leq 120$ MW (See Fig. 29). Then, we obtain $W_{div} > 5.3 / n_{20}^{0.4}$ MW/m^2, which means that n_e should be larger than 1×10^{20} m^{-3} in order to reduce the divertor heat load down to the level of ignition mode (5 MW/m^2). For this reason, the low divertor heat load (< 5 MW/m^2) is hardly compatible with the high controllability (>30 %). Figures 30 and 31 show the contour line plots of the controllability (I_{NBI}/I_P) at the operation point of the longest burn time and of 2000 s burn time, respectively. It is seen that I_{NBI}/I_P decreases from 63 % to 23 % at Point H_3 when the operation point is optimized by reducing the burn time. On the other hand, the divertor heat load decreases from 14.8 MW/m^2 to 7.3 MW/m^2 (Const-χ case) to make up for it. The best operation point is Point H_2, if the controllability must be larger than 30 %.

The controllability (I_{NBI}/I_P) of Point H_4 obtained in the previous section is 18 %. MHD safety factor at Point H_4 (4.8) is a little larger than that of Point H_1 (4.3) and Troyon g is smaller than the maximum value (3.0). These facts may lead to the relaxation of the requirement of controllability somewhat. It should be an important physics R & D how much controllability is required.

5. Conclusions and Summary

(i) Steady-state mode operations

Steady-state mode operations of ITER are investigated. There is an operation window when the fusion power P_{FUS} is less than about 750 MW. Here, we assume that $P_{NBI} \leq 120$ MW, Troyon g ≤ 3 and H ≤ 2.1. The maximum fusion power decreases down to about

690 MW when H ≤ 2.0 is assumed. The operation point is optimized with respect to divertor heat load. Three types of scaling models (Const-χ model, Bohm-χ model and JT-60U model) for peak divertor heat load are considered to include the uncertainty in the models. The divertor heat load is minimum at the lowest-I_P operation point for all scaling models. The dependence of the divertor heat load on the fusion power is similar for all models. The divertor heat load given by Const-χ model is, however, 1.8 times larger than that by Bohm-χ model when P_{FUS} = 750 MW. The highest fusion power differs greatly with each model when the allowable heat load is given. The possible highest fusion power is 200 ~ 400 MW when the maximum allowable heat load is the same as ignition mode operations (5 MW/m^2). Therefore, it is important to refine the divertor scaling model in the future physics R & D.

Several schemes to improve the divertor condition are also discussed. Divertor heat load can be reduced about 15 % by reducing the helium concentration from 10 % to 6 %. The heat load decreases by 20 ~ 25 % as H-factor increases from 2.0 to 2.2. Improvement of the current-drive efficiency γ is also effective. The divertor heat load decreases by 20 ~ 30 % as γ/γ_{ITER} increases from 1.0 to 1.4, where γ_{ITER} is the current-drive efficiency given by ITER guidelines. Impurity seeding is more effective. The heat load decreases to the level of ignition mode (~5 MW/m^2) when Fe concentration increases from 0.06 % to 0.28 %. In this case, however, Z_{eff} increases from 2.2 to 3.5 and P_{NBI} increases from 120 MW to 150 MW to compensate the enhanced radiation. Further study should be done experimentally, since the effect of the impurity seeding on the main plasma is uncertain. In this context, divertor cooling by seeding the impurities directly into the divertor region should be also critical in future works.

We also discuss the synergetic effect. It is found that the divertor heat load can be reduced to the level of the ignition mode without impurity seeding if we can assume that H = 2.5, g = 3.4, He = 5 % and the current-drive efficiency is enhanced by 40 %. Major operation points obtained in this report (including the reference point) are summarized as follows;

S_1 : Highest-P_{FUS} case for H=2.1 (P_{FUS}=750 MW : Reference point)
S_2 : Highest-P_{FUS} case for H=2.0 (P_{FUS}=690 MW)
S_3 : Lowest-W_{div} case for P_{FUS}=690 MW
(H_{IP}=2.1, He=10 %, g=2.9, P_{NBI}=120 MW, γ/γ_{ITER}=1.0)
S_4 : Lowest-W_{div} case for P_{FUS}=690 MW
(H_{IP}=2.5, He= 5 %, g=3.4, P_{NBI}=120 MW, γ/γ_{ITER}=1.4)
S_0 : Lowest-W_{div} case for P_{FUS}=690 MW [Offset-linear scaling]
(H_{IO}=2.0, He=10 %, g=3.6, P_{NBI}=120 MW, γ/γ_{ITER}=1.0)

Parameters of these operation points are listed in Table 4.

(ii) Hybrid mode operations

Hybrid mode operation appears to be suitable for the technology testing that requires long burn time and high neutron wall load simultaneously. The achievable burn time is calculated for the given fusion power and NBI current-drive power. It is found that NBI power should be larger than about 60 MW in order to obtain the burn time longer than 2000 s that is required for the technology testing. Here, we assume that $P_{NBI} \leq 120$ MW, $g \leq 3$ and $H \leq 2.0$. The divertor heat load is optimized by decreasing the burn time down to 2000 s when the achievable burn time is longer than 2000 s. It is found that the heat load is minimum when P_{NBI} is maximum and P_{FUS} is minimum. For P_{FUS} = 690 MW, the smallest divertor heat load (about 6 ~ 7 MW/m^2) is achieved when P_{NBI} = 110 MW (See Point H_3 in Table 5). The divertor heat load can be reduced to the level of the ignition mode (~5 MW/m^2) without impurity seeding by increasing H-factor from 2.0 to 2.2 (See Point H_4 in Table 5). The burn time is, however, 2000 s, while it is 2500 s for the reference point (Point H_1). In this case, the controllability (I_{NBI}/I_P) is about 18 %. MHD safety factor at Point H_4 is a little larger than that of Point H_1 and Troyon g is smaller than the critical value. This fact may lead to the relaxation of the requirement of controllability somewhat. It is an important R & D to investigate the required controllability quantitatively.

Divertor heat load at Point H_1 can be also reduced to the level

of the ignition mode without impurity seeding by reducing the burn time from 2500 s to 2000 s and keeping H = 2.2 (shown by Point H_5 in Table 5). H-factor should be increased to 2.3 to secure the burn time of 2500 s (see Point H_6 in Table 5). Major operation points obtained in this report (including the reference point) are summarized as follows;

H_1: Smallest-W_{div} with impurity seeding for H=2.2
(P_{FUS} = 860 MW, P_{NBI} = 110 MW : Reference point)
H_2: Case with the minimum-P_{FUS} (690 MW) for technology testing, the minimum-P_{NBI} (70 MW) for 2000 s and H=2.0
H_3: Smallest-W_{div} with 2000 s burning for H=2.0
(P_{FUS} = 690 MW, P_{NBI} = 110 MW)
H_4: Smallest-W_{div} with 2000 s burning for H=2.2
(P_{FUS} = 690 MW, P_{NBI} = 110 MW)
H_5: Smallest-W_{div} with 2000 s burning for H=2.2
(P_{FUS} = 860 MW, P_{NBI} = 110 MW)
H_6: Smallest-W_{div} with 2500 s burning for H=2.3
(P_{FUS} = 860 MW, P_{NBI} = 110 MW)

Parameters of these operation points are listed in Table 5.

Acknowledgements

The authors are grateful to Drs. Y. Shimomura and T. Tsunematsu for valuable discussions, and to Dr. S. Matsuda for continuous encouragement.

of the ignition mode without impurity seeding by reducing the burn time from 2500 s to 2000 s and keeping H = 2.2 (shown by Point H_5 in Table 5). H-factor should be increased to 2.3 to secure the burn time of 2500 s (see Point H_6 in Table 5). Major operation points obtained in this report (including the reference point) are summarized as follows;

H_1: Smallest-W_{div} with impurity seeding for H=2.2
(P_{FUS} = 860 MW, P_{NBI} = 110 MW : Reference point)
H_2: Case with the minimum-P_{FUS} (690 MW) for technology testing, the minimum-P_{NBI} (70 MW) for 2000 s and H=2.0
H_3: Smallest-W_{div} with 2000 s burning for H=2.0
(P_{FUS} = 690 MW, P_{NBI} = 110 MW)
H_4: Smallest-W_{div} with 2000 s burning for H=2.2
(P_{FUS} = 690 MW, P_{NBI} = 110 MW)
H_5: Smallest-W_{div} with 2000 s burning for H=2.2
(P_{FUS} = 860 MW, P_{NBI} = 110 MW)
H_6: Smallest-W_{div} with 2500 s burning for H=2.3
(P_{FUS} = 860 MW, P_{NBI} = 110 MW)

Parameters of these operation points are listed in Table 5.

Acknowledgements

The authors are grateful to Drs. Y. Shimomura and T. Tsunematsu for valuable discussions, and to Dr. S. Matsuda for continuous encouragement.

References

[1] L. J. Perkins and ITER Physics Group, *"ITER document series, No. 22"*, IAEA/ITER/DS/22, IAEA, Vienna (1991).

[2] T. Nakazato *et. al.*, *"Study on operational capability of ITER"*, JAERI-M 91-209 (1991).

[3] N. A. Uckan and ITER Physics Group, *"ITER document series, No. 10"*, IAEA/ITER/DS/10, IAEA, Vienna (1990).

[4] N. Fujisawa, *"Bootstrap current and neutral beam current drive"*, ITER-IL-PH-6-9-J-1 (1989).

[5] K. Itami *et. al.*, *"Characteristics of Divertor Plasma and Scrape-off Layer in JT-60U"*, in *Proc. 10th Intl. Conf. on Plasma-Surface Interactions in Contr. Fusion Devices*, Monterey, USA, J. Nucl. Mater. (1992).

[6] M.F.A. Harrison and E. Hotston, in *Proc. 9th Intl. Conf. on Plasma-Surface Interactions in Contr. Fusion Devices*, Bournemouth, UK, J. Nucl. Mater. (1990).

[7] S-I. Itoh *et. al.*, Plasma Physics and Controlled Fusion, **32** (1990) 415.

[8] D. E. Post and ITER Physics Group, *"ITER Document series, No. 21"*, IAEA/ITER/DS/21, IAEA, Vienna (1991).

Table 1 Major plasma parameters and design parameters.

Major radius	R_P	(m)	6.0
Minor radius	a_P	(m)	2.15
Aspect ratio	A		2.79
Elongation	κ_{95}		2.0
Triangularity	δ_{95}		0.35
Elongation at separatrix	κ_x		2.22
Triangularity at separatrix	δ_x		0.518
Plasma volume	V_P	(m^3)	1070
Plasma surface area	S_P	(m^2)	880
Plasma current	I_P	(MA)	25 / 22
MHD safety factor	q_Ψ		2.7 / 3.0
Plasma self-inductance	L_P	(μH)	9.24
Toroidal field on axis	B_T	(T)	4.85
Maximum toroidal field	B_{TMAX}	(T)	11.2
Position of maximum field	R_{TFC}	(m)	2.72
TF coil stored energy		(GJ)	42
Maximum poloidal field	B_{PMAX}	(T)	13.4
Position of OH coils	R_{OH}	(m)	1.725
PF coil stored energy		(GJ)	15 / 12
Weight		(ton)	28400

Table 2 Parameters of ITER reference operation points.

			Ignition (I_1)	Steady-state (S_1)	Hybrid (H_1)
Electron temperature	T_e	(keV)	10	20	11
Electron density	n_e	($10^{20}/m^3$)	1.22	0.64	1.06
Plasma current	I_P	(MA)	22.0	18.9	15.4
Bootstrap current	I_{BS}	(MA)	3.3	5.4	4.7
NBI current	I_{NBI}	(MA)	-	13.5	4.4
OH current	I_{OH}	(MA)	18.7	-	6.3
MHD safety factor	q_ψ		3.0	3.5	4.3
Cylindrical q	q_{cyl}		2.5	2.9	3.5
Engineering q	q_I		2.1	2.5	3.0
Troyon coefficient	g		2.0	3.0	2.7
Toroidal beta	β_t	(%)	4.2	5.4	4.0
Poloidal beta	β_p		0.65	1.1	1.4
Effective ion charge	Z_{eff}		1.66	2.16	2.17
Helium accumulation	He	(%)	10	10	10
Impurity seeding (Fe)	f_{seed}	(%)	-	-	0.07
Fusion power	P_{FUS}	(MW)	1080	750	860
Neutron wall load	L_{wal}	(MW/m^2)	1.0	0.7	0.8
Fusion gain	Q		∞	6.7	7.9
Alpha heating power	P_α	(MW)	216	150	172
Ohmic power	P_{OH}	(MW)	2	-	1
NBI power	P_{NBI}	(MW)	-	115	110
Bremsstrahlung loss	P_{BR}	(MW)	49	25	50
Line radiation loss	P_{LIN}	(MW)	14	7	35
Synchrotron loss	P_{SYN}	(MW)	4	16	5
Convection loss	W_p/τ_E	(MW)	151	217	193
Confinement time	τ_E	(s)	3.8	2.7	2.7
H-factor	H_{IP} / H_{IO}		2.0/1.9	2.1/1.7	2.2/1.8
Radiation loss in SOL	P_{EDGE}	(MW)	35	27	95
Power to SOL	P_{div}	(MW)	116	190	98
Divertor temperature	T_{div}	(eV)	28	640	30
Divertor heat load	W_{div}	(MW/m^2)	5	17	4
Total flux	Φ_{total}	(Vs)	325	324	314
Flux for current-rize	Φ_{ramp}	(Vs)	270	232	189
Flux for burn	Φ_{burn}	(Vs)	45	82	115
Loop voltage	V_{loop}	(V)	0.114	-	0.046
Pulse duration	T_{burn}	(s)	400	∞	2500

Table 3 Plasma parameters of steady-state mode at the boundary of operation region when P_{FUS} = 450 MW. It is seen that the divertor heat load W_{div} is smallest at Point A for all models.

		A	B	C
I_P	(MA)	13.1	22.0	22.0
T_e	(KeV)	12.3	23.4	21.2
n_e	($10^{20}m^{-3}$)	0.69	0.50	0.52
g		2.6	2.3	2.2
H_{IP}		2.1	2.1	1.8
P_{NBI}	(MW)	120	107	120
$W_{div}^{Const-\chi}$	(MW/m^2)	9.1	11.9	13.9
$W_{div}^{Bohm-\chi}$	(MW/m^2)	6.4	8.0	8.9
W_{div}^{JT-60U}	(MW/m^2)	6.6	8.9	10.4

Table 4 Parameters of Steady-state mode operations.

		(S_1)	(S_2)	(S_3)	(S_4)	(S_0)
P_{FUS}	(MW)	750	690	←	←	←
L_{wal}	(MW/m^2)	0.7	0.6	←	←	←
T_e	(keV)	20	18.9	15.7	7.4	8.3
n_e	(10^{20}/m^3)	0.64	0.63	0.70	1.21	1.20
I_P	(MA)	18.9	19.0	15.8	10.1	10.0
q_ψ		3.5	3.5	4.2	6.6	6.7
P_{NBI}	(MW)	115	120	←	←	←
γ / γ_{ITER}		1.0	←	←	1.4	1.0
I_{NBI}/I_P		0.71	0.74	0.68	0.39	0.32
η_{NBI}	(A/W)	0.121	0.116	0.090	0.033	0.027
Q		6.7	5.7	←	←	←
Troyon g		3.0	2.8	2.9	3.4	3.6
H_{IP}		2.1	2.0	2.1	2.5	2.8
H_{IO}		1.7	1.6	1.6	1.8	2.0
He	(%)	10	←	←	5	10
Z_{eff}		2.16	2.17	2.04	1.56	1.66
Impurity seeding	(%)	No	←	←	←	←
P_{MAIN}	(MW)	47	45	43	57	63
P_{EDGE}	(MW)	25	25	26	34	35
P_{div}	(MW)	190	190	189	166	159
T_{div}	(eV)	640	650	480	64	59
$W_{div}^{Const-\chi}$	(MW/m^2)	17	17	14	6	6
$W_{div}^{Bohm-\chi}$	(MW/m^2)	10	10	9	5	5
W_{div}^{JT-60U}	(MW/m^2)	13	13	11	5	5
V_{loop}	(V)	0.0	←	←	←	←
T_{burn}	(s)	∞	←	←	←	←

Table 5 Parameters of Hybrid mode operations.

		(H_1)	(H_2)	(H_3)	(H_4)	(H_5)	(H_6)
P_{FUS}	(MW)	860	690	←	←	860	←
L_{wal}	(MW/m^2)	0.8	0.6	←	←	0.8	←
T_e	(keV)	10.6	14.6	8.8	7.7	7.8	7.9
n_e	($10^{20}/m^3$)	1.06	0.72	1.12	1.31	1.44	1.41
I_P	(MA)	15.4	18.9	15.1	14.0	14.3	13.7
q_ψ		4.3	3.5	4.4	4.8	4.6	4.9
P_{NBI}	(MW)	110	70	110	←	←	←
γ / γ_{ITER}		1.0	←	←	←	←	←
I_{NBI}/I_P		0.29	0.30	0.23	0.18	0.16	0.18
η_{NBI}	(A/W)	0.041	0.081	0.031	0.023	0.021	0.022
Q		7.9	9.9	6.3	←	7.8	←
Troyon g		2.7	2.2	2.4	2.6	2.8	2.9
H_{IP}		2.2	2.0	←	2.2	←	2.3
H_{IO}		1.8	←	1.6	1.8	1.7	1.8
He	(%)	10	←	←	←	←	←
Z_{eff}		2.17	1.98	1.69	1.64	1.62	1.62
Impurity seeding	(%)	0.07	No	←	←	←	←
P_{MAIN}	(MW)	90	43	58	69	79	77
P_{EDGE}	(MW)	95	26	33	37	40	39
P_{div}	(MW)	98	139	157	142	163	166
T_{div}	(eV)	30	210	72	35	35	40
$W_{div}^{Const-\chi}$	(MW/m^2)	3.7	9.3	7.3	5.3	6.2	6.4
$W_{div}^{Bohm-\chi}$	(MW/m^2)	3.8	6.9	6.0	4.9	5.4	5.4
W_{div}^{JT-60U}	(MW/m^2)	3.3	7.5	6.4	4.9	5.8	5.8
V_{loop}	(V)	0.046	0.039	0.058	0.065	0.063	0.053
T_{burn}	(s)	2500	2000	←	←	←	2500

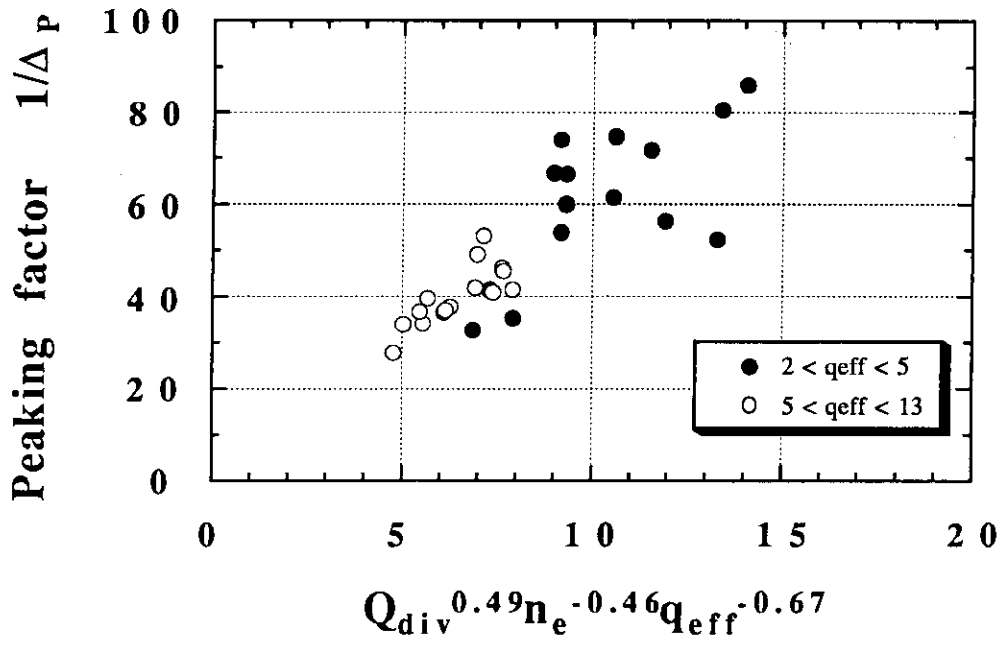

Fig. 1 Empirical scaling law for the peaking factor in JT-60U [5]. Here, $1/\Delta_p$ (m^{-1}) is the peaking factor, Q_{div} (MW) is the power to the scrape off layer, n_e ($10^{19}/m^3$) is the average electron density and q_{eff} is the effective safety factor, respectively.

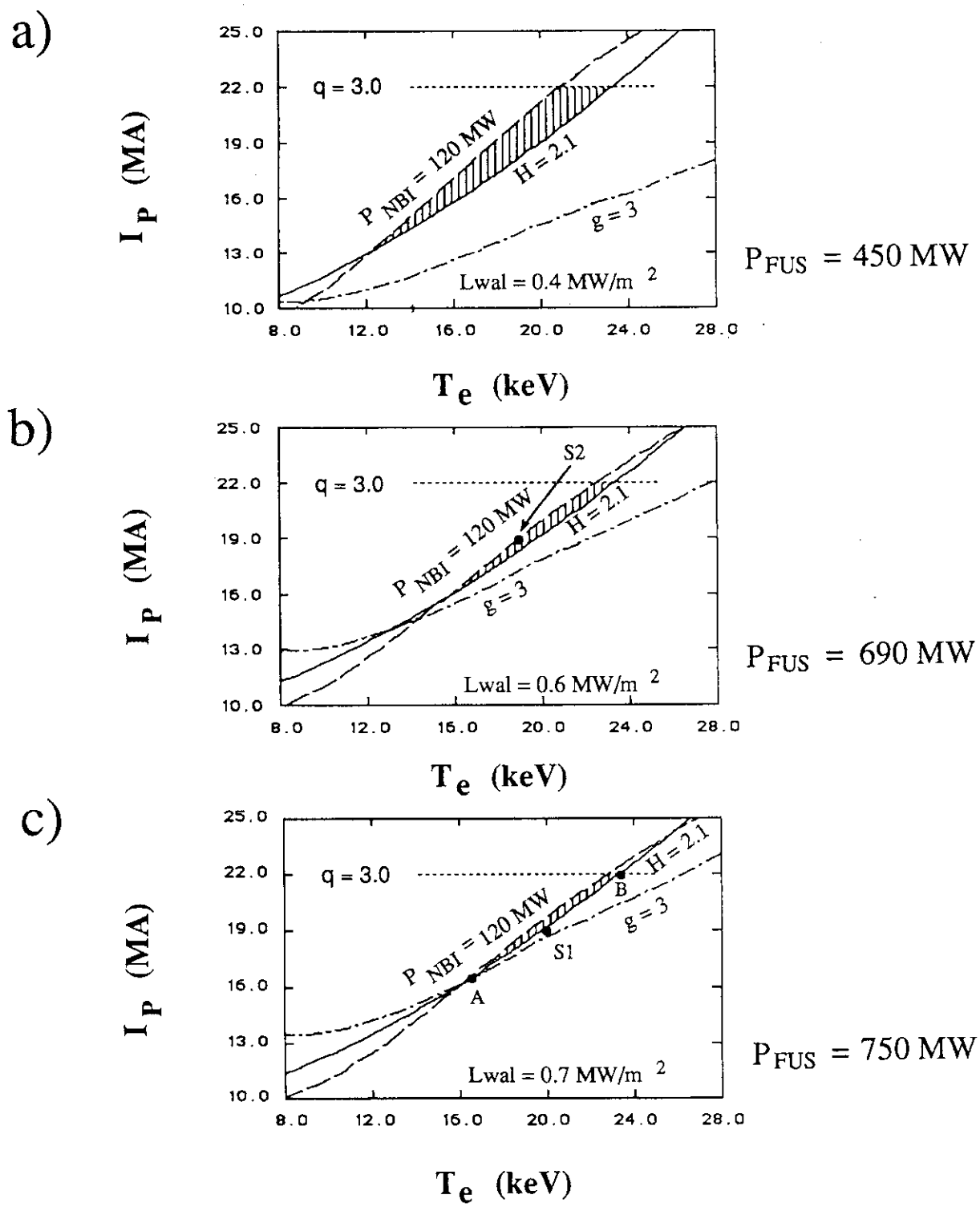

Fig. 2 Steady-state operation region of ITER for ITER-89 power scaling law.

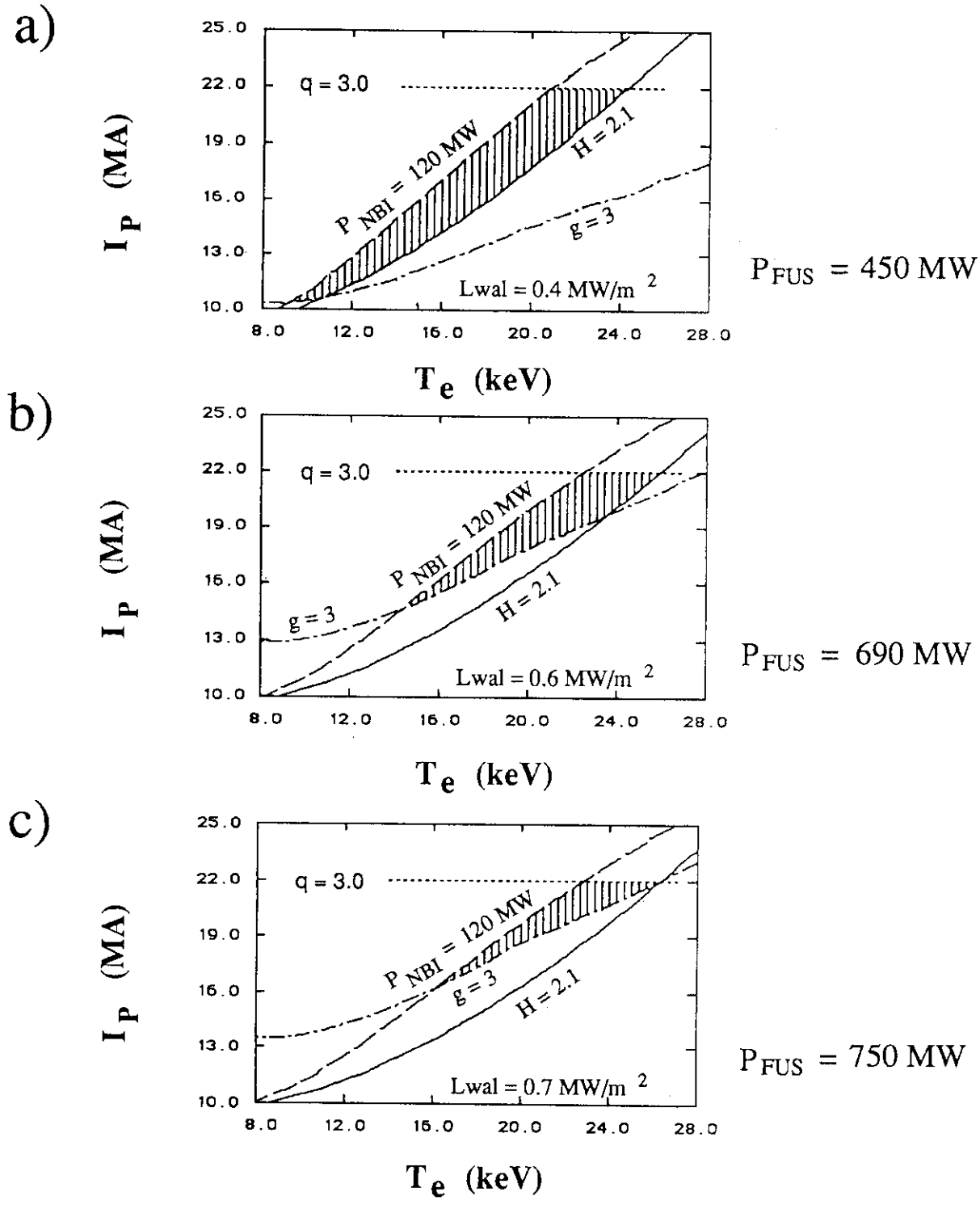

Fig. 3 Steady-state operation region of ITER for ITER-89 offset-linear scaling law.

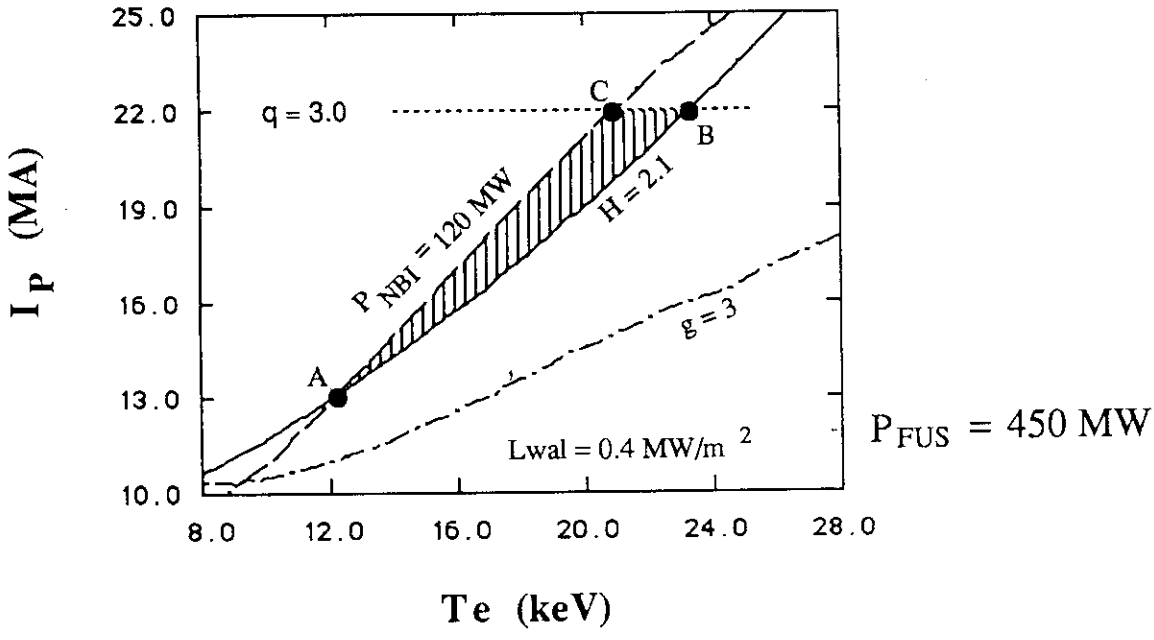

Fig. 4 Steady-state operation region for $L_{Wal} = 0.4$ MW/m^2.

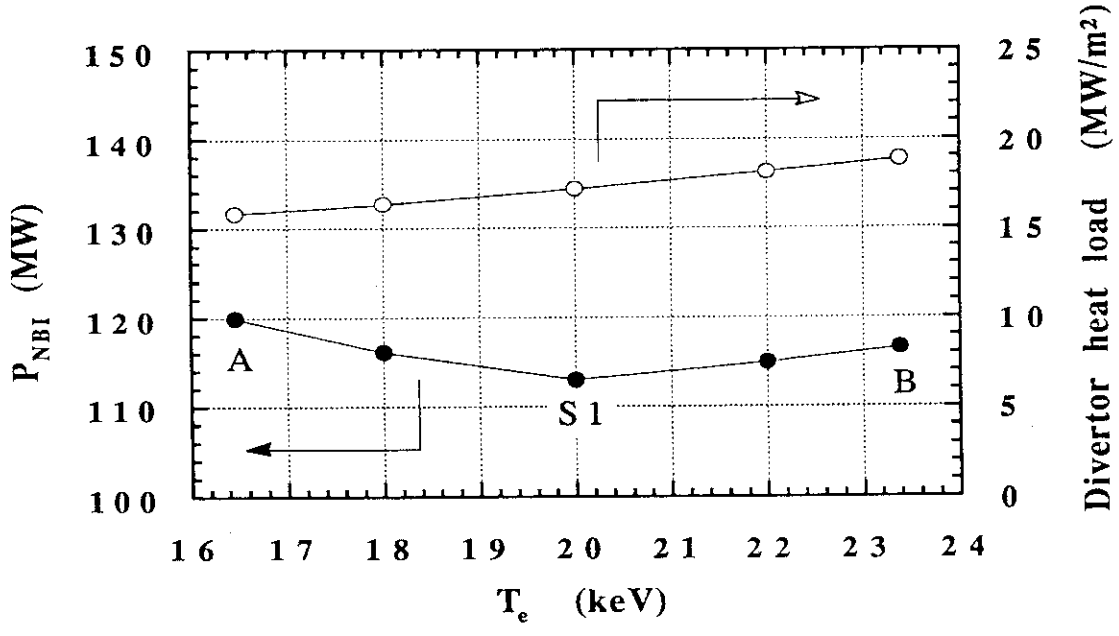

Fig. 5 Current-drive power and the divertor heat load when $L_{Wal} = 0.7$ MW/m^2 ($P_{FUS} = 750$ MW).

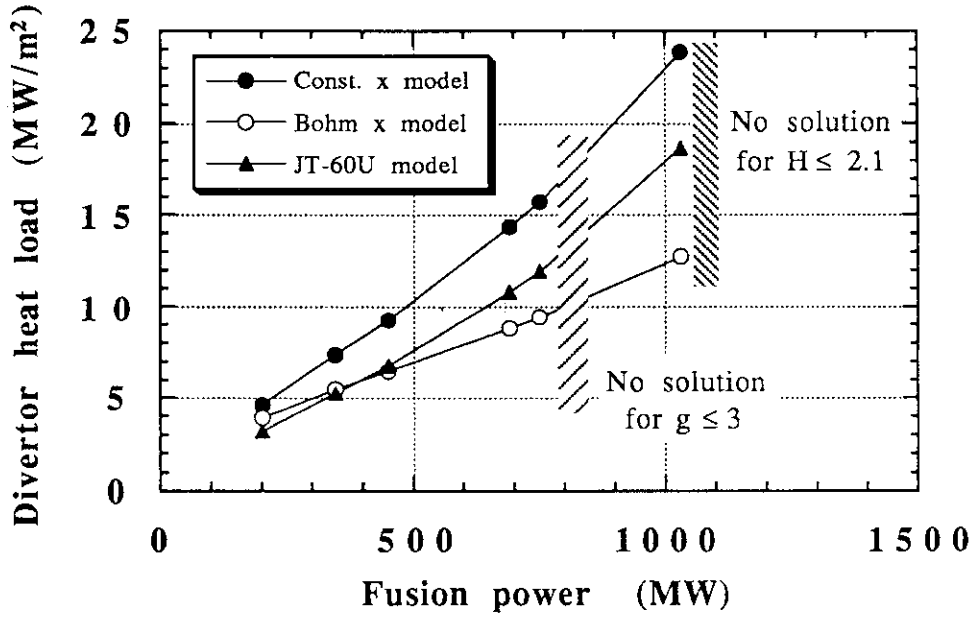

Fig. 6 Divertor heat load of steady-state mode at Point A for various fusion powers. Here, ITER-89 power scaling law is assumed.

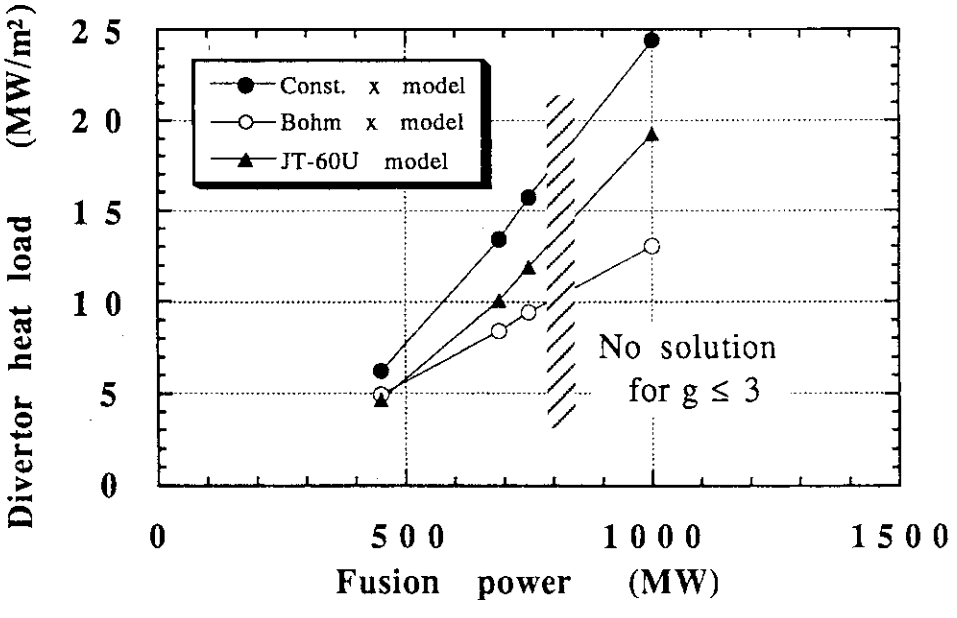

Fig. 7 Divertor heat load of steady-state mode at Point A for various fusion powers. Here, ITER-89 offset-linear scaling law is assumed.

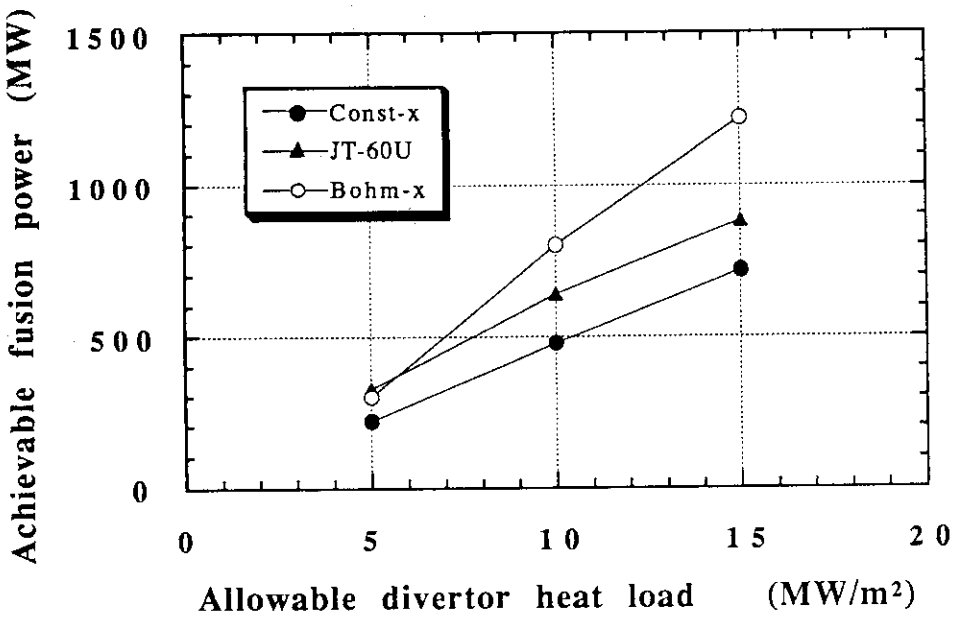

Fig. 8 Maximum fusion power of steady-state mode as a function of the allowable divertor heat load for various models. Here, ITER-89 power scaling law is used.

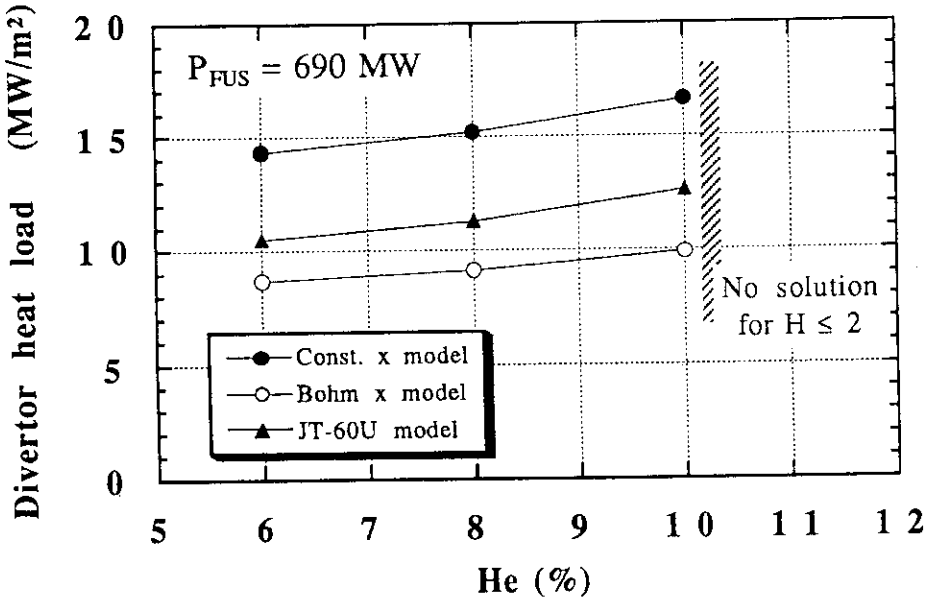

Fig. 9 Divertor heat load of steady-state mode as a function of helium concentration for P_{FUS} = 690 MW. Here, P_{NBI} = 120 MW, H = 2, g ≤ 3 and ITER-89 power scaling law is used.

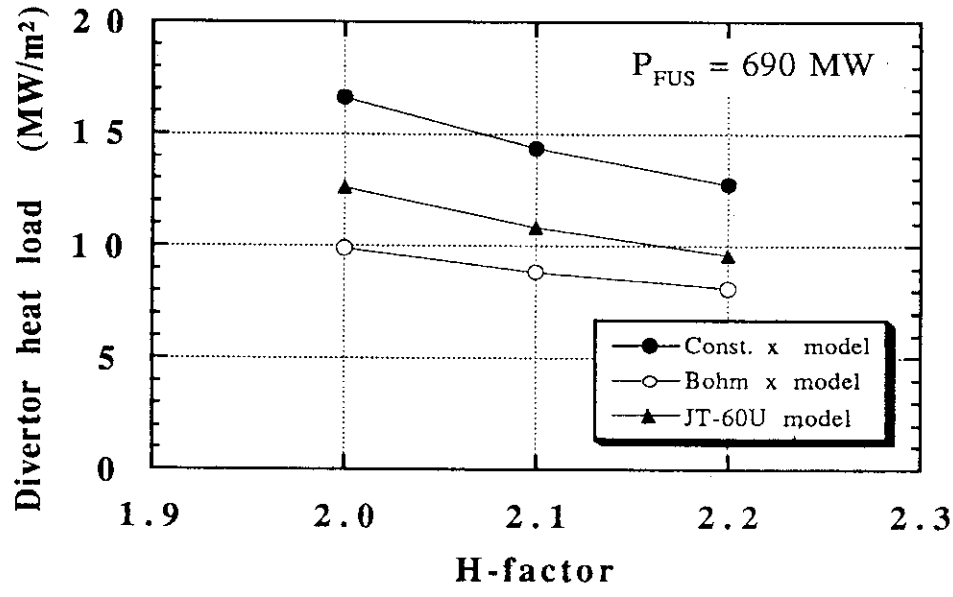

Fig. 10 Divertor heat load of steady-state mode as a function of H-factor when P_{FUS} = 690 MW. Here, P_{NBI} = 120 MW, g ≤ 3, He = 10% and ITER-89 power scaling law is assumed.

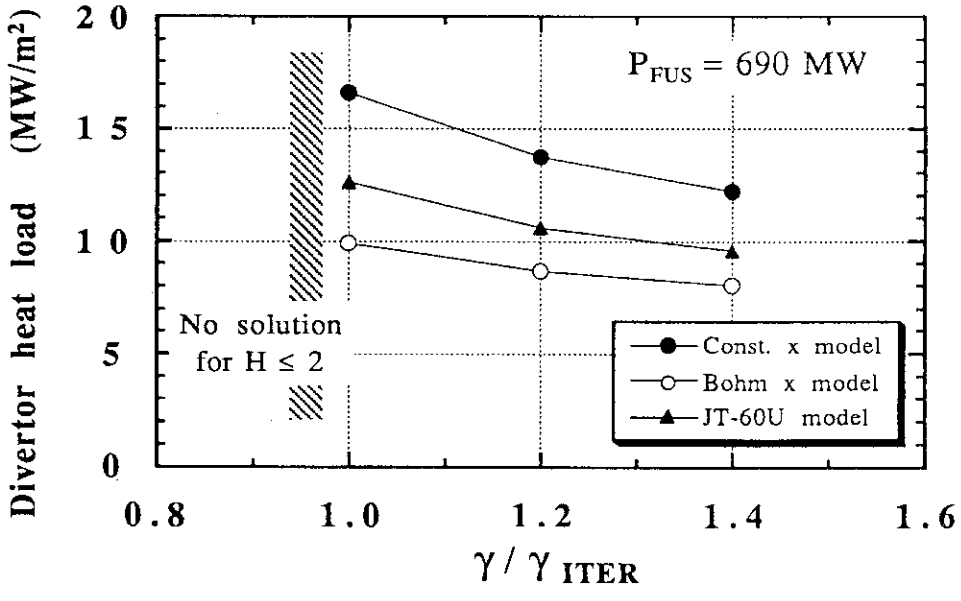

Fig. 11 Divertor heat load of steady-state mode as a function of current-drive efficiency γ normalized by γ_{ITER} when P_{FUS} = 690 MW. Here, γ_{ITER} is the current-drive efficiency given by ITER guidelines, H = 2.0 and ITER-89 power scaling law is assumed.

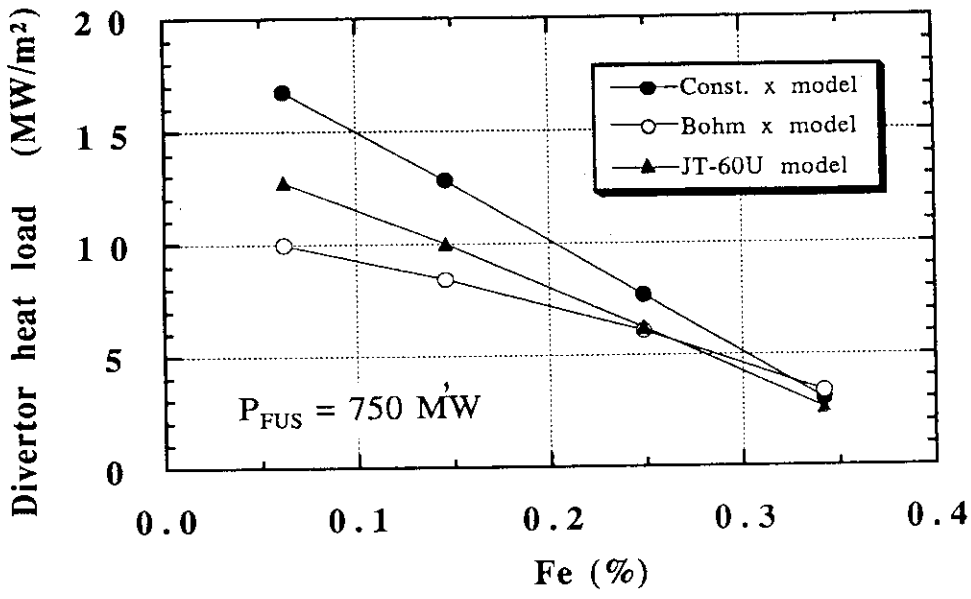

Fig. 12 Divertor heat load of steady-state mode as a function of Fe concentration when P_{FUS} = 750 MW. Here, H = 2.1, $g \leq 3$ and ITER-89 power scaling law is assumed.

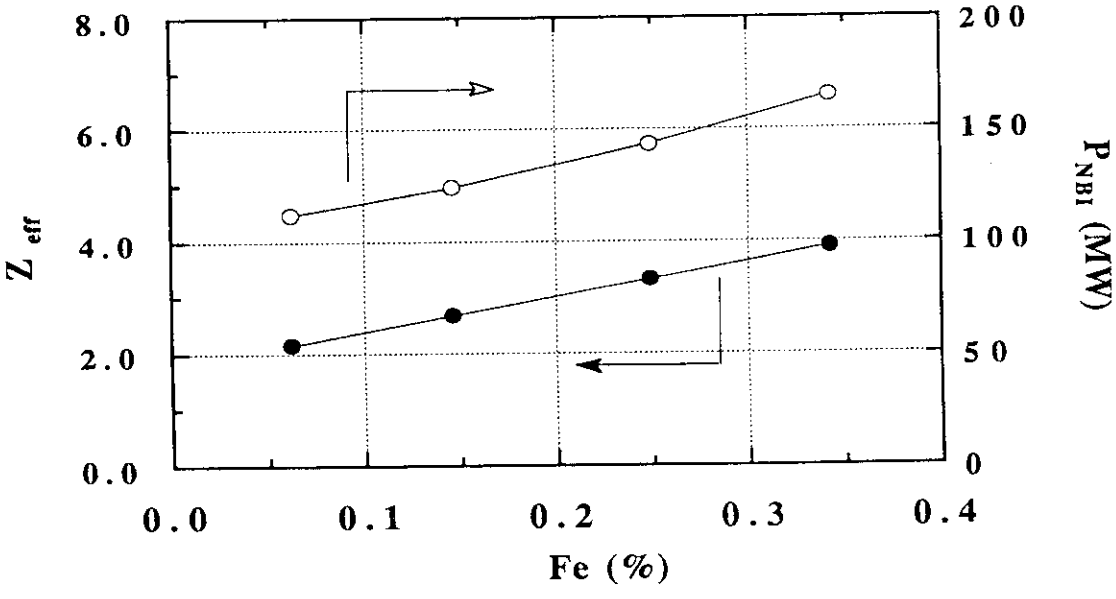

Fig. 13 Effective ion charge and required current-drive power corresponding to Fig. 12. Here, H = 2.1, $g \leq 3$ and ITER-89 power scaling law is assumed.

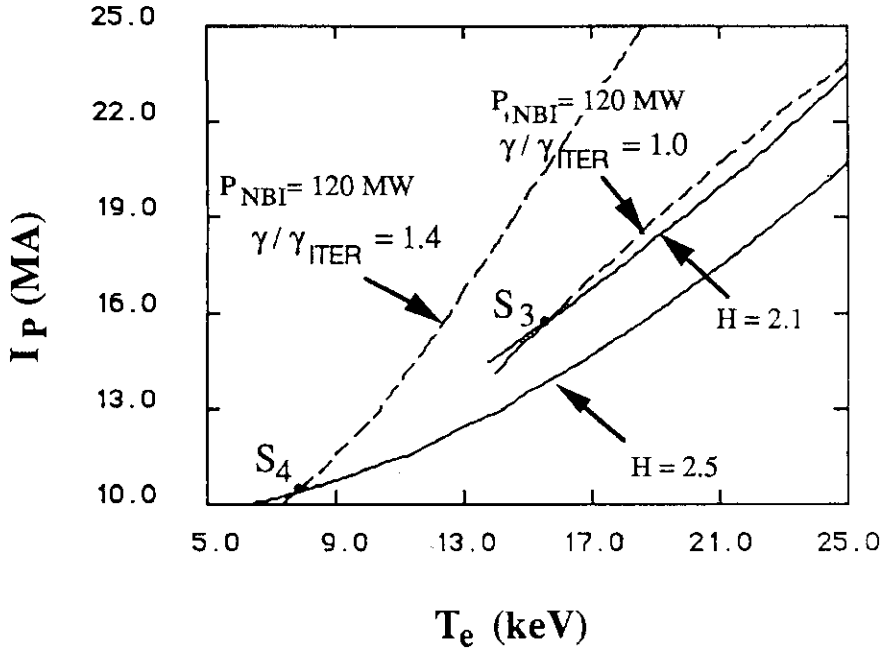

Fig. 14 Steady-state operation region of ITER when P_{FUS} = 690 MW. Here, solid lines and dashed lines denote the contours of H-factor and P_{NBI}, respectively. In this figure, ITER-89 power scaling law is assumed.

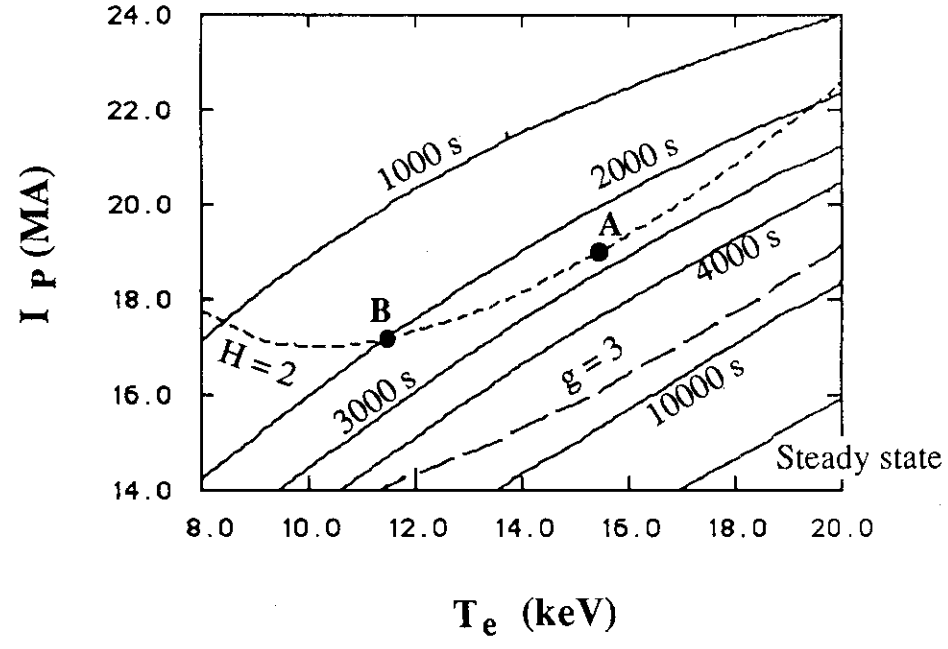

Fig. 15 Hybrid operation region of ITER when P_{FUS} = 860 MW and P_{NBI} = 80 MW. Here, solid lines, dotted line and dashed line denote the contours of burn time, H-factor and Troyon g, respectively. In this figure, ITER-89 power scaling law is assumed.

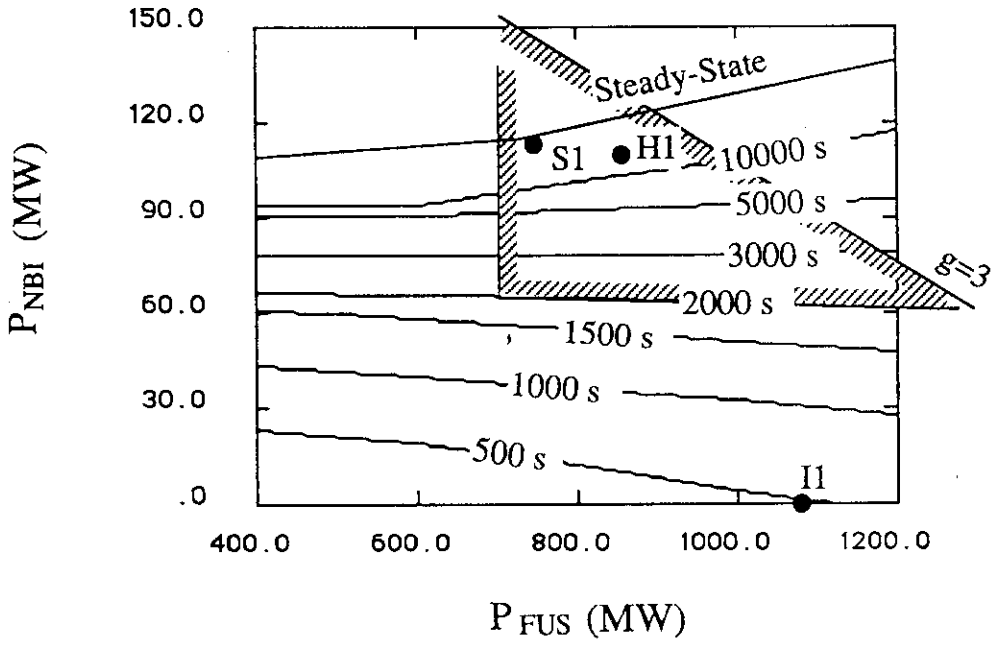

Fig. 16 Achievable longest burn time in P_{NBI}-P_{FUS} space. Here, H = 2 and $g \leqq 3$.

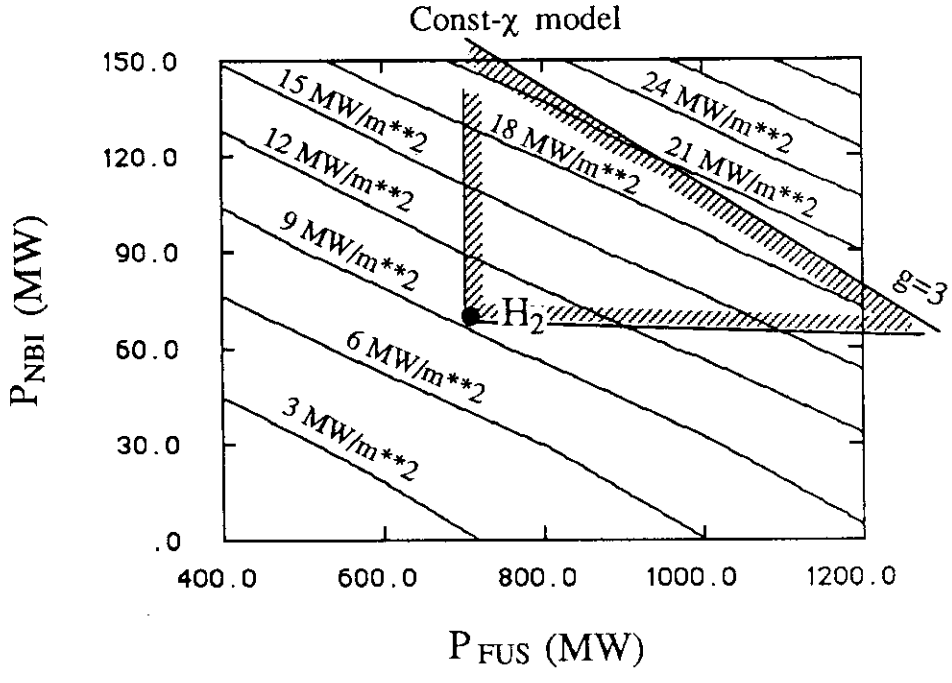

Fig. 17 Divertor heat load at the operation point of the longest burn time (Const-χ model).

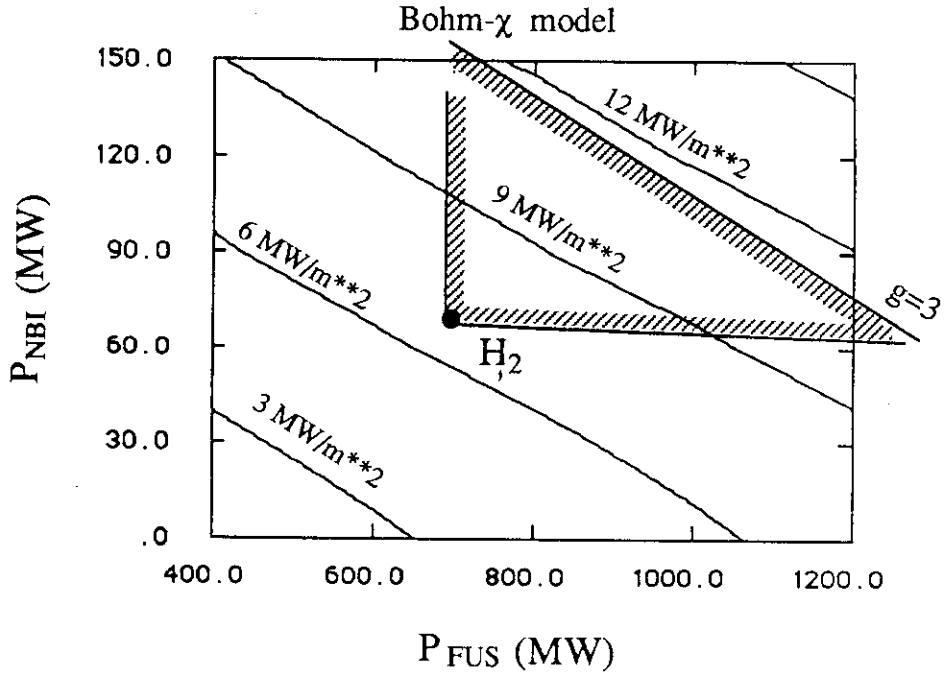

Fig. 18 Divertor heat load at the operation point of the longest burn time (Bohm-χ model).

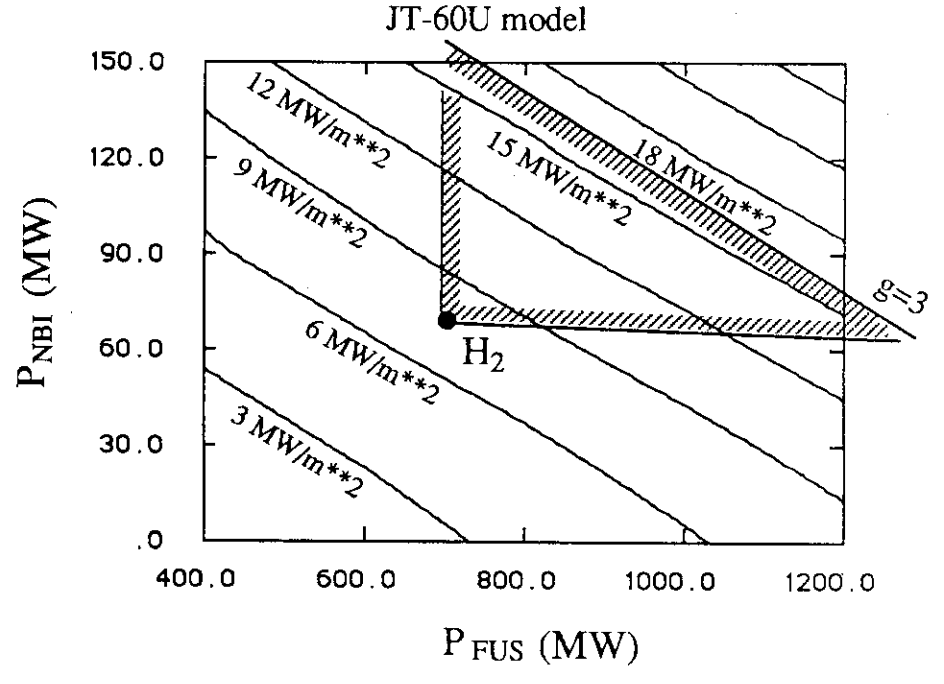

Fig. 19 Divertor heat load at the operation point of the longest burn time (JT-60U model).

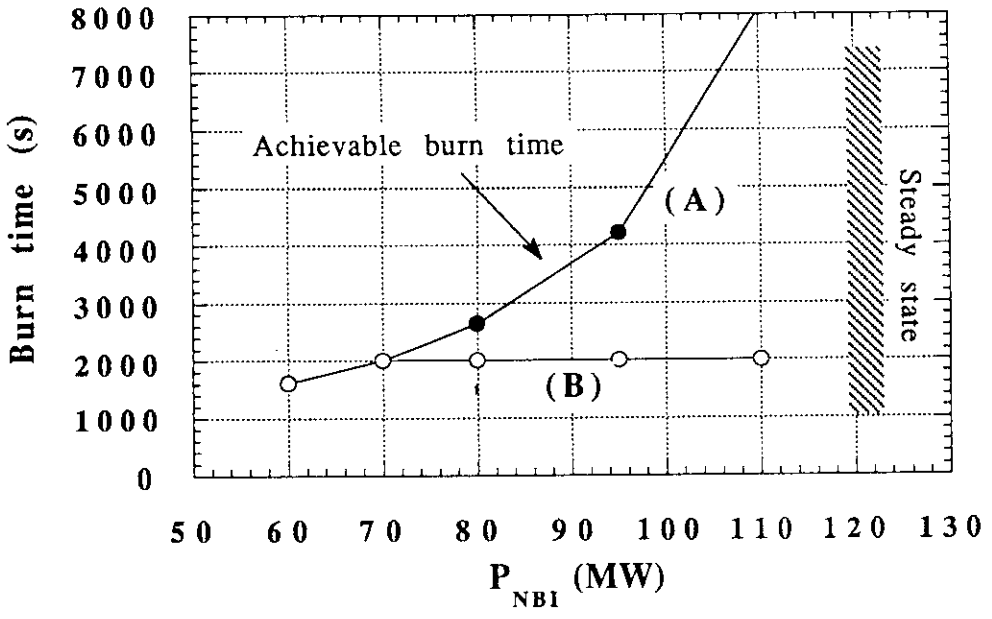

Fig. 20 Burn time at Point A and Point B for various P_{NBI} when P_{FUS} = 860 MW. Here, H = 2, g < 3 and ITER-89 power scaling law is assumed.

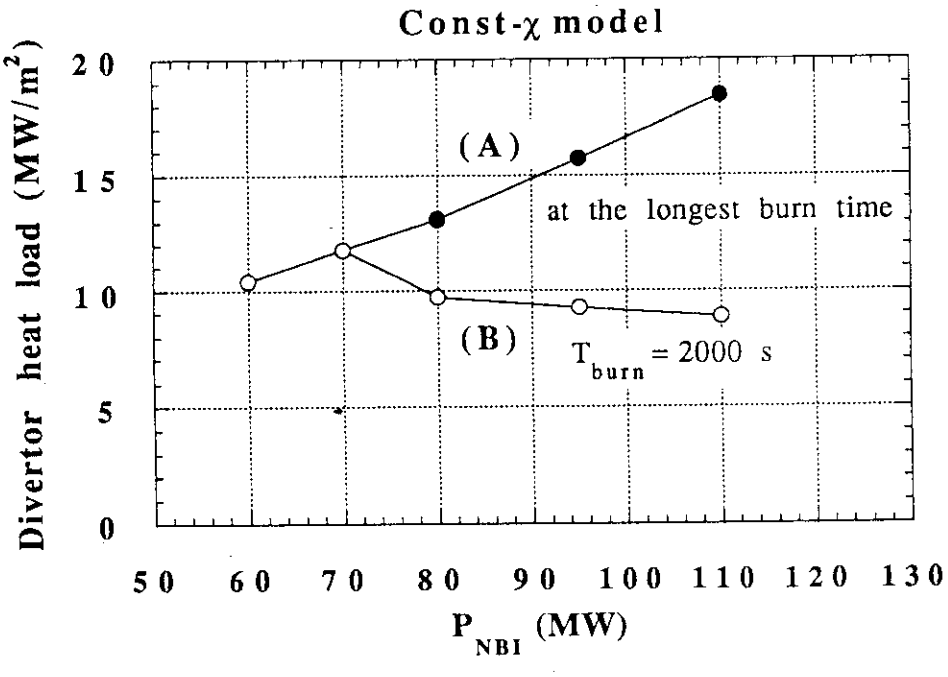

Fig. 21 Divertor heat load (Const-χ model) at the longest burn time and at 2000 s for P_{FUS} = 860 MW.

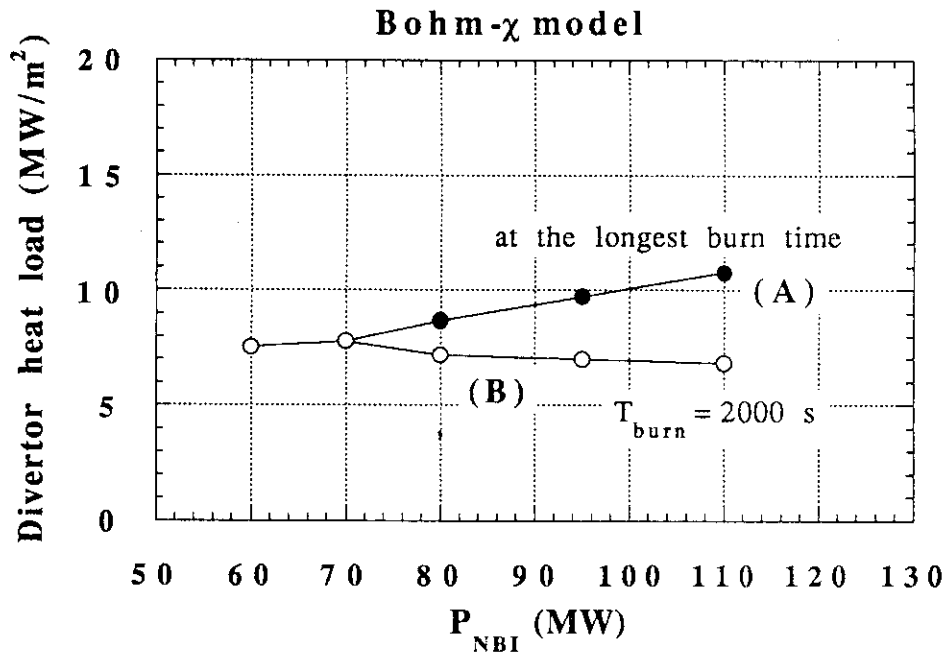

Fig. 22 Divertor heat load (Bohm-χ model) at the longest burn time and at 2000 s for P_{FUS} = 860 MW.

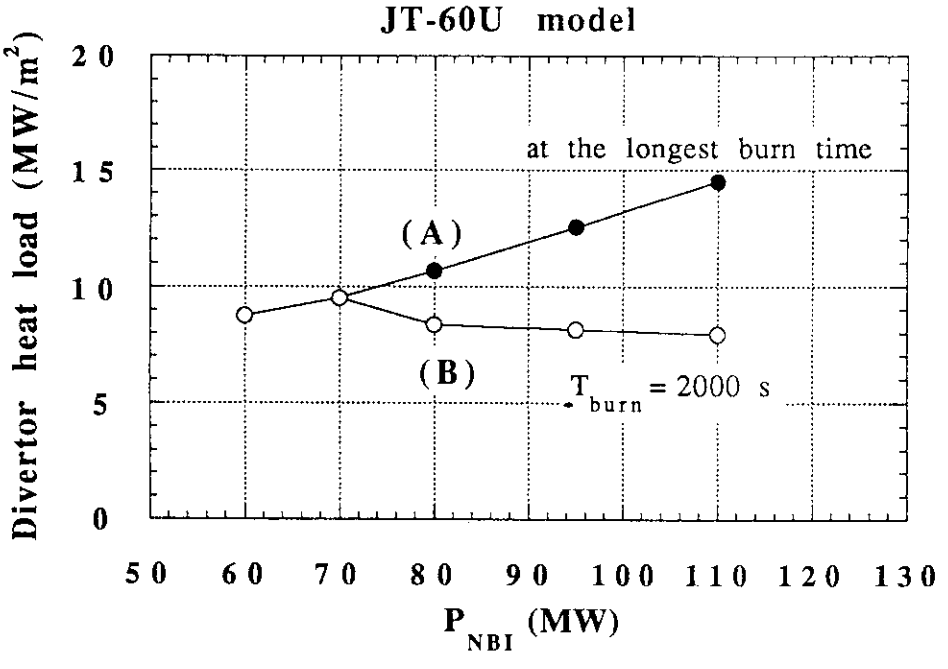

Fig. 23 Divertor heat load (JT-60U model) at the longest burn time and at 2000 s for P_{FUS} = 860 MW.

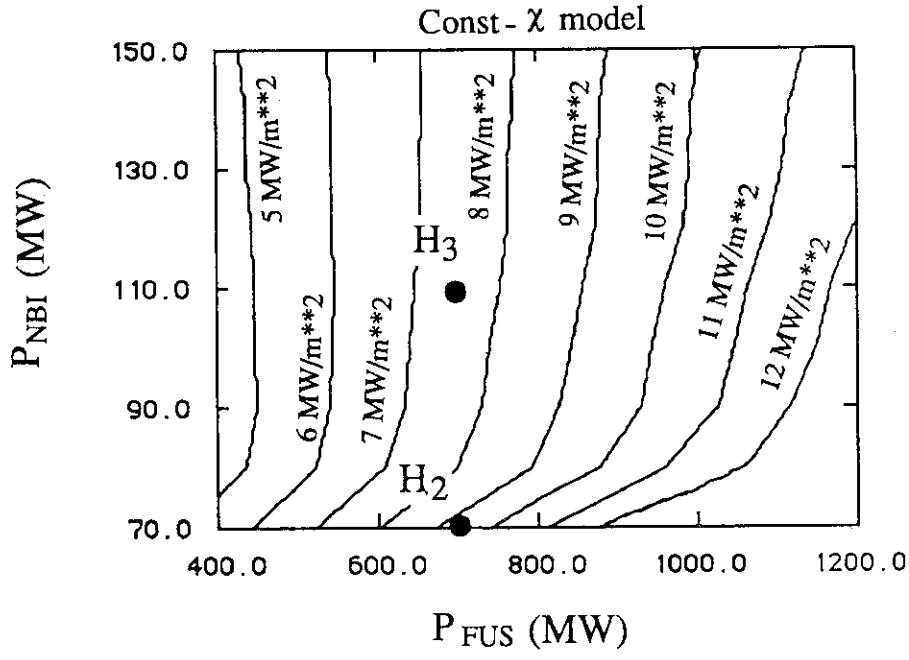

Fig. 24 Divertor heat load at 2000 s burn (Const-χ model).

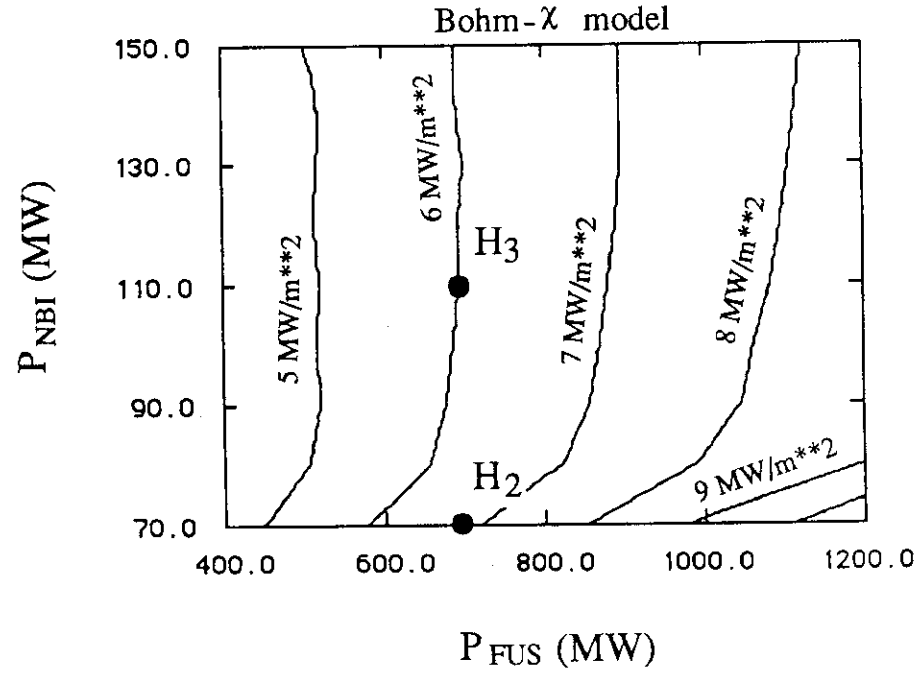

Fig. 25 Divertor heat load at 2000 s burn (Bohm-χ model).

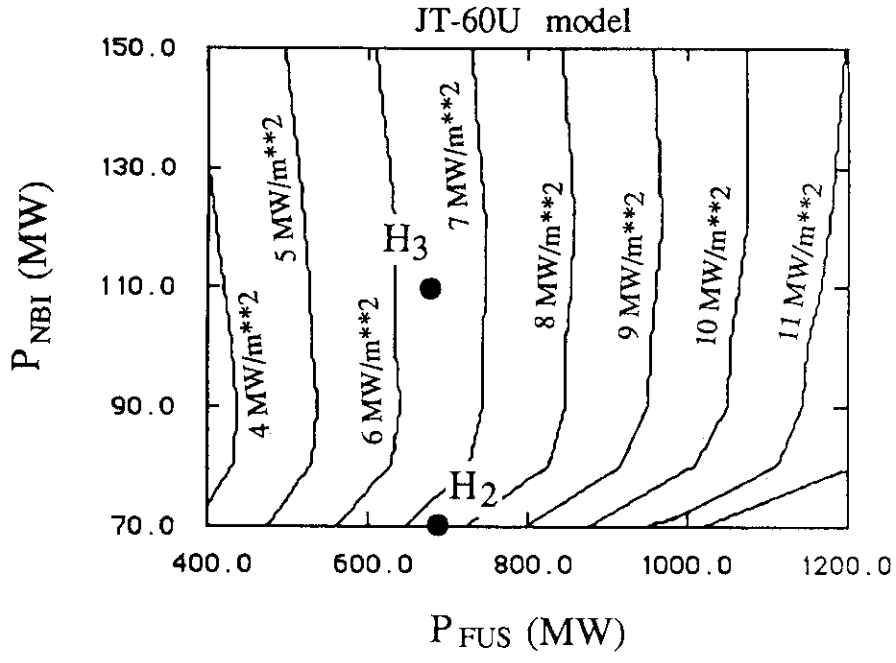

Fig. 26 Divertor heat load at 2000 s burn (JT-60U model).

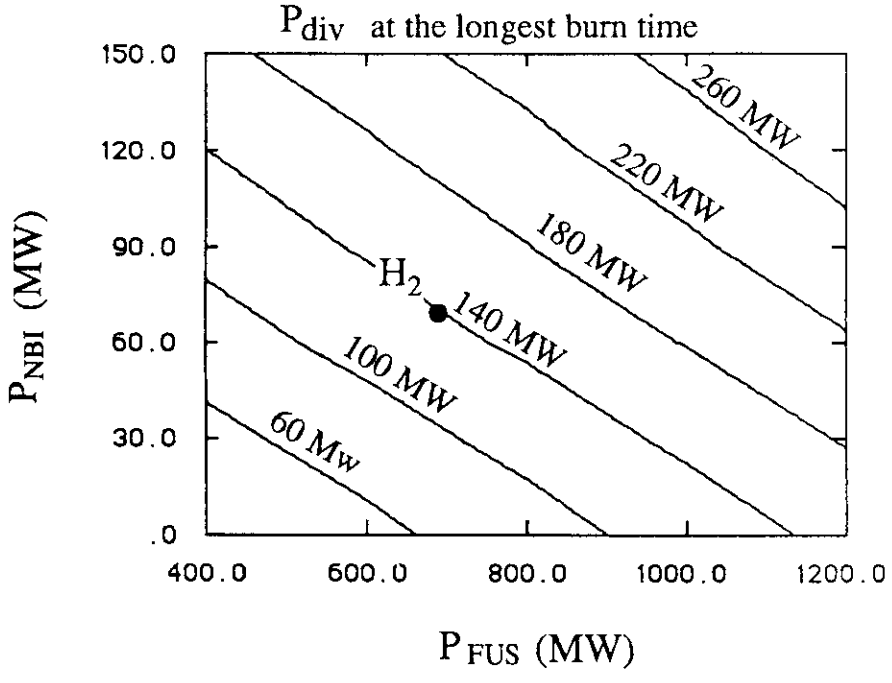

Fig. 27 Power to the divertor region at the operation point with the longest burn time.

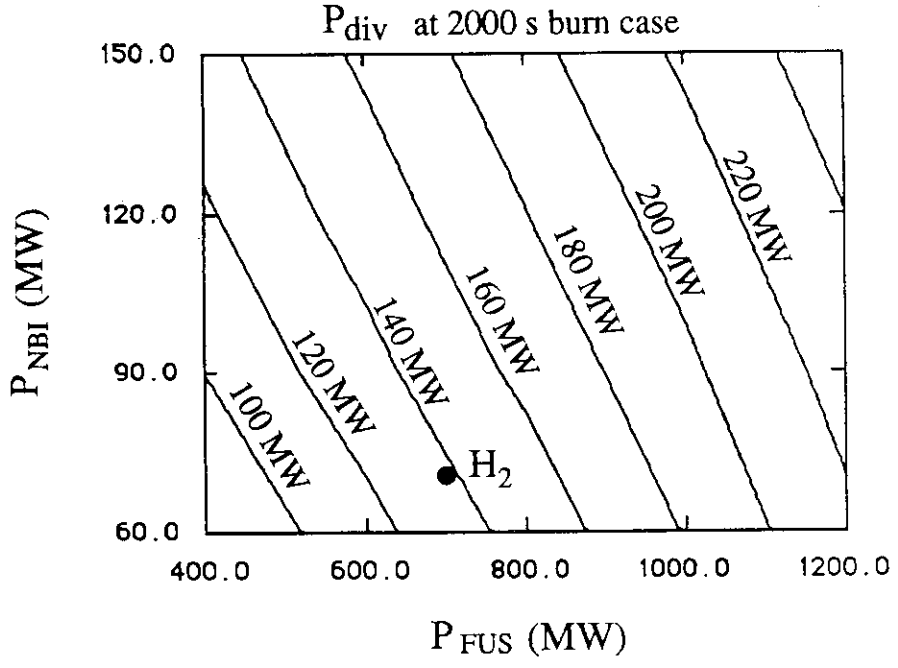

Fig. 28 Power to the divertor region at the operation point with the burn time of 2000 s.

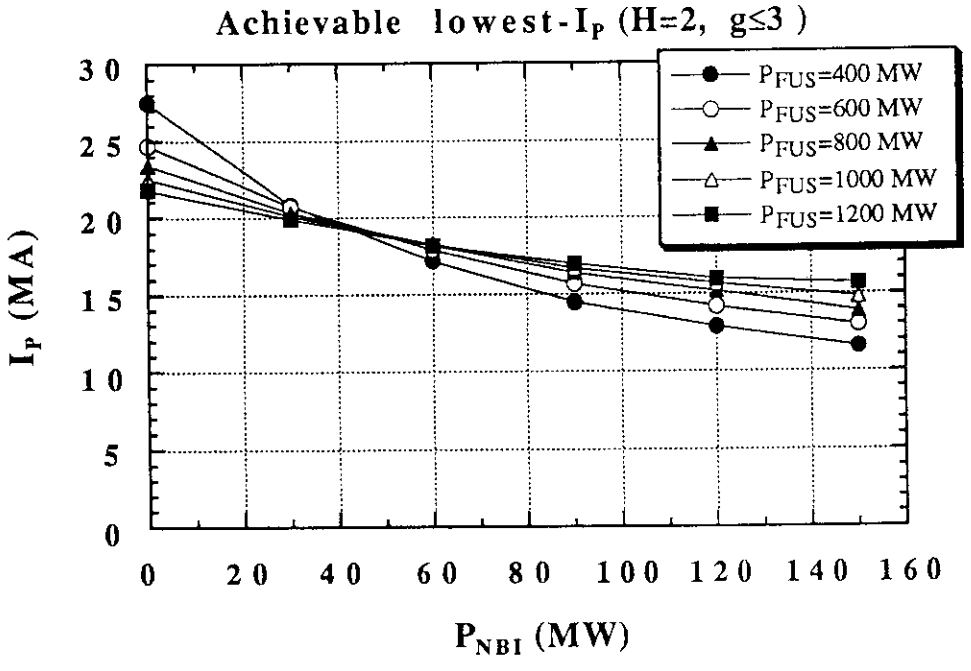

Fig. 29 Achievable lowest-I_p when H = 2 and g ≤ 3.

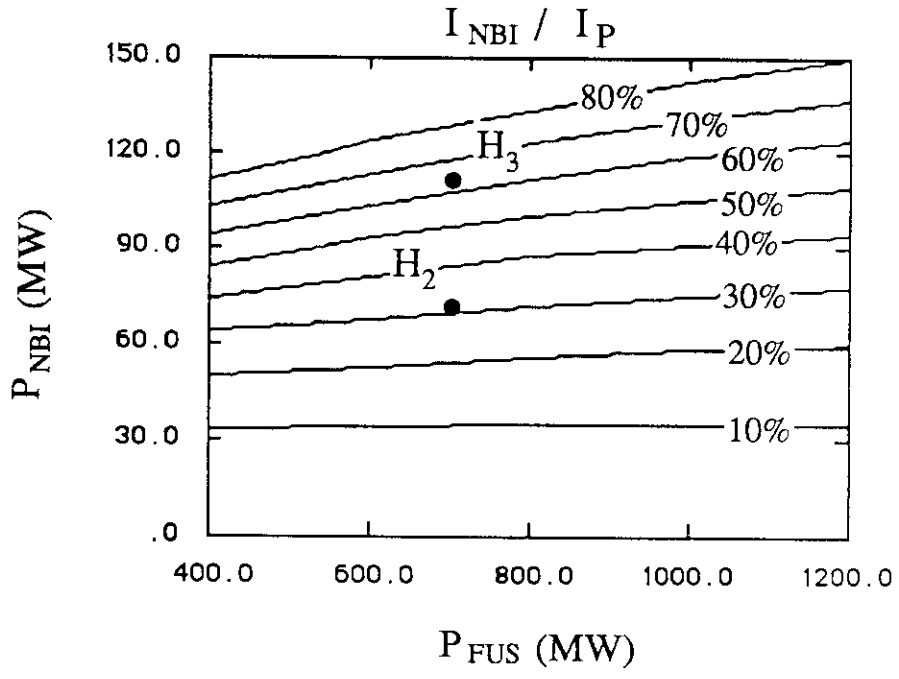

Fig. 30 Controllability at the operation point with the longest burn time.

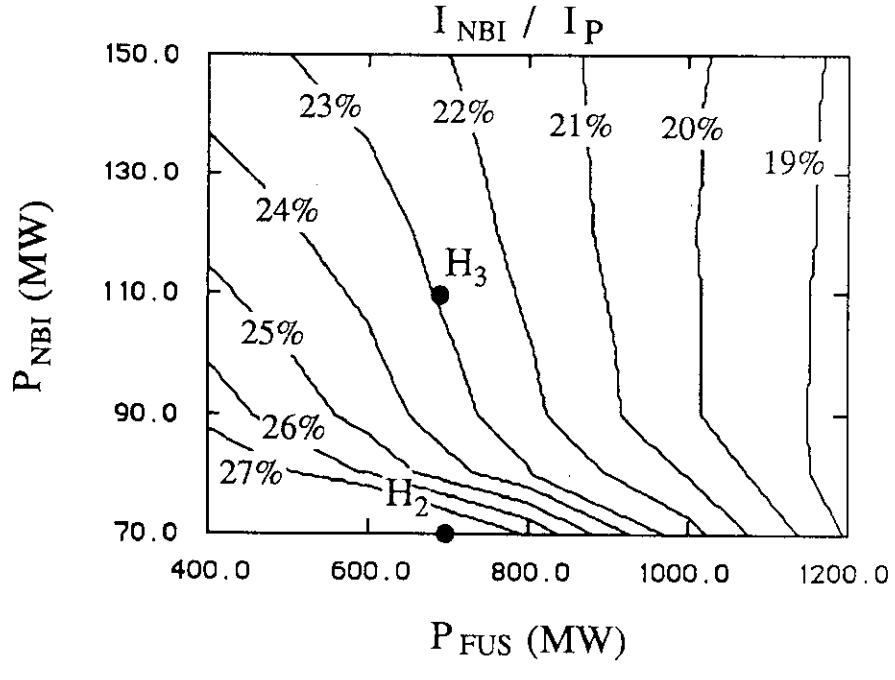

Fig. 31 Controllability at the operation point with the burn time of 2000 s.